Intervalence Transfer at the Localized-to-Delocalized, Mixed-Valence Transition in Osmium Polypyridyl Complexes

Konstantinos D. Demadis,[†] Gregory A. Neyhart,[‡] Edward M. Kober,[‡] Peter S. White,[‡] and Thomas J. Meyer*,[‡]

Venable and Kenan Laboratories, Department of Chemistry, CB 3290, The University of North Carolina at Chapel Hill, Chapel Hill, North Carolina 27599-3290, and Global Water Research, Nalco Chemical Company, One Nalco Center, Naperville, Illinois 60563-1198

Received July 1, 1999

The mixed-valence complexes $[(bpy)_2(Cl)Os^{III}(BL)Os^{II}(Cl)(bpy)_2]^{3+}$ and $[(tpy)(bpy)Os^{III}(BL)Os^{II}(bpy)(tpy)]^{5+}$ (bpy is bipyridine; tpy is 2,2′:6′,2″-terpyridine; BL is a bridging ligand, either 4,4′-bipyridine (4,4′-bpy) or pyrazine (pz)) have been prepared and studied by infrared and near-infrared measurements in different solvents. For BL = 4,4′-bpy, there is clear evidence for localized Os^{II} and Os^{III} oxidation states in the appearance of the expected two interconfigurational $d\pi \rightarrow d\pi$ bands at Os^{III} and additional, broad absorption features in the near-infrared arising from intervalence transfer (IT) transitions. For $[(bpy)_2(Cl)Os(pz)Os(Cl)(bpy)_2]^{3+}$ and $[(tpy)(bpy)Os(pz)Os(bpy)(tpy)]^{5+}$, unusually intense ν(pz) bands appear in the infrared at 1599 cm^{-1} (ϵ = 2600 M^{-1} cm^{-1}) for the former and at 1594 cm^{-1} (ϵ = 2020 M^{-1} cm^{-1}) for the latter. They *provide an oxidation state marker and evidence for localized oxidation states.* A series of bands appear in the near-infrared from 2500 to 8500 cm^{-1} that can be assigned to a combination of interconfigurational $d\pi \rightarrow d\pi$ and IT transitions. In CD_3CN, in the mid-infrared, bands arising from ν(bpy) ring stretching modes from 1400 to 1500 cm^{-1} are averaged for $[(bpy)_2(Cl)Os(pz)Os(Cl)(bpy)_2]^{3+}$ or significantly perturbed for $[(tpy)(bpy)Os(pz)Os(bpy)(tpy)]^{5+}$ compared to electronically isolated Os^{II} and Os^{III} complexes. The pyrazine-bridged complexes have properties that place them in a new class of mixed-valence molecules, Class II−III having properties associated with both Class II and Class III in the Robin and Day classification scheme. The characteristic features of this class are that oxidation states are localized because of vibrational coupling but that solvent orientational motions are uncoupled because of rapid intramolecular electron transfer.

Introduction

In the classification scheme of Robin and Day, mixed-valence complexes can be grouped as class I (localized oxidation states, no interaction), class II (localized, with an interaction), and class III (delocalized).[1] If localized, the odd electron is in an orbital on one site, at least on a time scale relevant to the nuclear motions coupled to electron transfer. If delocalized, the odd electron is in a molecular orbital delocalized over both sites, and it is not possible to assign integral oxidation states.

In either case, bands typically appear at low energy in the near-infrared region of the spectrum.[1,2] With localization, they arise from charge transfer (or intervalence transfer, IT) transitions in which light absorption results in electron transfer between orbitals on different sites. These bands are typically of low intensity because of weak electronic coupling and are broad because of coupling with the solvent.[2] For transition metal complexes, there are multiple IT transitions because of the effect of low symmetry and spin−orbit coupling on the d orbitals. This leads to multiple IT bands which, if not separately resolved, also contribute to the bandwidth.[3] With delocalization, the low-energy bands arise from transitions between molecular orbitals (from symmetric to antisymmetric combinations of metal and bridging ligand orbitals) and the bands are intense and narrow.[4−6]

The general properties of mixed-valence complexes are reasonably well understood. Theoretical models have been developed to explain their behavior.[1,2,4−6] However, direct

* Corresponding author. E-mail: tjmeyer@email.unc.edu.
[†] Nalco Chemical Co.
[‡] The University of North Carolina.

(1) (a) Robin, M. B.; Day, P. *Adv. Inorg. Chem. Radiochem.* **1967**, *10*, 247. (b) Prassides, K., Ed. *Mixed Valence Systems: Applications in Chemistry, Physics and Biology*; Kluwer Academic Publishers: Dordrecht, The Netherlands, 1990. (c) Taube, H. *Pure Appl. Chem.* **1976**, *44*, 25. (d) Meyer, T. J. *Acc. Chem. Res.* **1978**, *11*, 94. (e) Brown, D. B., Ed. *Mixed Valence Compounds*; D. Reidel Publishing Co.: Dordrecht, The Netherlands, 1980. (f) Day, P. *Int. Rev. Phys. Chem.* **1981**, *1*, 149. (g) Seddon, K. R. *Coord. Chem. Rev.* **1982**, *41*, 79. (h) Hush N. S. *Prog. Inorg. Chem.* **1967**, *8*, 391. Hush, N. S. *Electrochim. Acta* **1968**, *13*, 1005. Hush, N. S. *Coord. Chem. Rev.* **1985**, *64*, 135.

(2) (a) Creutz, C. *Prog. Inorg. Chem.* **1983**, *30*, 1. (b) Hush, N. *Coord. Chem. Rev.* **1985**, *64*, 135. (c) Creutz, C.; Newton, M. D.; Sutin, N. *J. Photochem. Photobiol., A* **1994**, *82*, 47. (d) Sutin, N. In *Electron Transfer in Inorganic, Organic and Biological Systems*; Bolton, J. R., Mataga, N., McLendon, G., Eds.; Advances in Chemistry Series, No. 228; American Chemical Society: Washington, DC, 1991; p 25. (e) Hush, N. S. *Electrochim. Acta* **1968**, *13*, 1005. (f) Tanner, M.; Ludi, A. *Inorg. Chem.* **1981**, *20*, 2348. (g) Grutchley, R. J. *Adv. Inorg. Chem.* **1994**, *41*, 273.

(3) (a) Kober, E. M.; Goldsby, K. A.; Narayana, D. N. S.; Meyer, T. J. *J. Am. Chem. Soc.* **1983**, *105*, 4303. (b) Chen, P.; Meyer, T. J. *Chem. Rev.* **1998**, *98*, 1439. (c) Powers, M. J.; Meyer, T. J. *J. Am. Chem. Soc.* **1980**, *102*, 1289.

(4) (a) Piepho, S. B. *J. Am. Chem. Soc.* **1990**, *112*, 4197. (b) Piepho, S. B. *J. Am. Chem. Soc.* **1988**, *110*, 6319. (c) Petrov, V.; Hupp, J. T.; Mottley, C.; Mann, L. C. *J. Am. Chem. Soc.* **1994**, *116*, 2171. (d) Wong, K. Y.; Schatz, P. N. *Prog. Inorg. Chem.* **1981**, *28*, 369. (e) Meyer, Y. J. *Ann. N.Y. Acad. Sci.* **1978**, *313*, 496. (f) Reimers, J. R.; Hush, N. S. *Chem. Phys.* **1996**, *208*, 177.

(5) (a) Piepho, S. B.; Krausz, E.; Schatz, P. N. *J. Am. Chem. Soc.* **1978**, *100*, 2996. (b) Neuenschwander, K.; Piepho, S. B.; Schatz, P. N. *J. Am. Chem. Soc.* **1985**, *107*, 7862. (c) Prassides, K.; Schatz, P. N. *J. Phys. Chem.* **1989**, *93*, 83. (d) Ondrechen, M. J.; Gozashoti, S.; Zheng, L. T.; Zhou, F. *Adv. Chem. Ser.* **1990**, *226*, 225. (e) Zheng, L. T.; Ko, J.; Ondrechen, M. J. *J. Am. Chem. Soc.* **1987**, *109*, 1666. (f) Broo, A.; Larsson, S. *Chem. Phys.* **1992**, *161*, 363.

(6) Dubicki, L.; Ferguson, J.; Krausz, E. R.; Lay, P. A.; Maeder, M.; Magnuson, R. H.; Taube, H. *J. Am. Chem. Soc.* **1985**, *107*, 2167.

10.1021/ic9907765 CCC: $18.00
Published on Web 12/10/1999

evaluation of the factors involved in determining whether localization or delocalization occurs has been somewhat elusive, and there are a growing number of examples that appear to exist at the interface between the two limiting descriptions. Well-defined examples of class II and class III behavior are well-known. For *cis,cis*-$[(bpy)_2(Cl)Ru^{III}(pz)Ru^{II}(Cl)(bpy)_2]^{3+}$ (bpy = 2,2′-bipyridine, pz = pyrazine), the UV−visible spectrum is essentially the sum of the Ru^{II} and Ru^{III} components except for a broad band appearing in the near-infrared at 7690 cm^{-1} (ϵ = 455) in CD_3CN which arises from three overlapping IT transitions.[3] For $[(NH_3)_5Os^{II.5}(N_2)Os^{II.5}(NH_3)_5]^{5+}$, a series of near-infrared bands appear arising from transitions between delocalized molecular levels.[6] For others, the descriptions that have been advanced are ambiguous, the most famous being the Creutz−Taube ion, $[(NH_3)_5Ru(pz)Ru(NH_3)_5]^{5+}$. It is difficult to describe the known properties of this complex satisfactorily by either localized or delocalized descriptions.[2,4−8] In *cis*-$[(bpy)_2(Cl)Os(pz)Ru(NH_3)_5]^{4+}$, the oxidation state distribution and, with it, the extent of electronic delocalization vary with solvent.[8] In the $Os^{III}-Ru^{II}$ isomer, there is significant electronic coupling but localized oxidation states. The transferring electron at Ru^{II} is in an orbital orthogonal to the bridge. In *trans,trans*-$[(tpy)(Cl)_2Os^{III}(N_2)Os^{II}(Cl)_2(tpy)]^+$, there are localized oxidation states, as shown by crystallography and the appearance of ν(N≡N) in the IR, but the solvent is not coupled to intramolecular electron transfer and IT bands are narrow and solvent independent.[9]

In this paper, we report results from a continuing investigation on the localized-to-delocalized, mixed-valence transition in Os mixed-valence complexes.[9] Part of this work has appeared in a preliminary communication.[10]

Experimental Section

The ligand-bridged cations relevant to the present study are listed in Chart 1, and the polypyridyl ligands are illustrated in Figure 1.

Abbreviations used in the text include BL = bridging ligand, pz = pyrazine, bpy = bipyridine, tpy = 2,2′:6′,2″-terpyridine, TFMS = trifluoromethane sulfonate, MLCT = metal-to-ligand charge transfer, and IT = intervalence transfer. In complexes $\mathbf{1}^{2+/3+/4+}$ and $\mathbf{2}^{2+/3+/4+}$, the bpy ligands are in a cis configuration.

Materials. Acetonitrile (Fisher, HPLC grade), toluene (Fisher, ACS Certified grade), ethanol (Fisher, 95%), and house-distilled water were all used without further purification. Alumina, ethylene glycol (ACS Certified grade), and anhydrous diethyl ether (ACS Certified grade) were all obtained from Fisher Scientific and used as received. Acetonitrile-d_3, trifluoromethanesulfonic acid, NH_4PF_6, 4,4′-bipyridine, pyrazine, and $(NH_4)_2[Ce(NO_3)_6]$ were obtained from Aldrich Chemical Co. and used as received. Neutral alumina was used as the support for column chromatography (unless otherwise noted) with a CH_3CN/toluene mixture as the eluant.

Chart 1

$[(bpy)_2(Cl)Os(4,4'\text{-}bpy)Os(Cl)(bpy)_2]^{2+}$	$\mathbf{1}^{2+}$
$[(bpy)_2(Cl)Os(4,4'\text{-}bpy)Os(Cl)(bpy)_2]^{4+}$	$\mathbf{1}^{4+}$
$[(bpy)_2(Cl)Os(4,4'\text{-}bpy)Os(Cl)(bpy)_2]^{3+}$	$\mathbf{1}^{3+}$
$[(bpy)_2(Cl)Os(pz)Os(Cl)(bpy)_2]^{2+}$	$\mathbf{2}^{2+}$
$[(bpy)_2(Cl)Os(pz)Os(Cl)(bpy)_2]^{4+}$	$\mathbf{2}^{4+}$
$[(bpy)_2(Cl)Os(pz)Os(Cl)(bpy)_2]^{3+}$	$\mathbf{2}^{3+}$
$[(tpy)(bpy)Os(4,4'\text{-}bpy)Os(bpy)(tpy)]^{4+}$	$\mathbf{3}^{4+}$
$[(tpy)(bpy)Os(4,4'\text{-}bpy)Os(bpy)(tpy)]^{6+}$	$\mathbf{3}^{6+}$
$[(tpy)(bpy)Os(4,4'\text{-}bpy)Os(bpy)(tpy)]^{5+}$	$\mathbf{3}^{5+}$
$[(tpy)(bpy)Os(pz)Os(bpy)(tpy)]^{4+}$	$\mathbf{4}^{4+}$
$[(tpy)(bpy)Os(pz)Os(bpy)(tpy)]^{6+}$	$\mathbf{4}^{6+}$
$[(tpy)(bpy)Os(pz)Os(bpy)(tpy)]^{5+}$	$\mathbf{4}^{5+}$

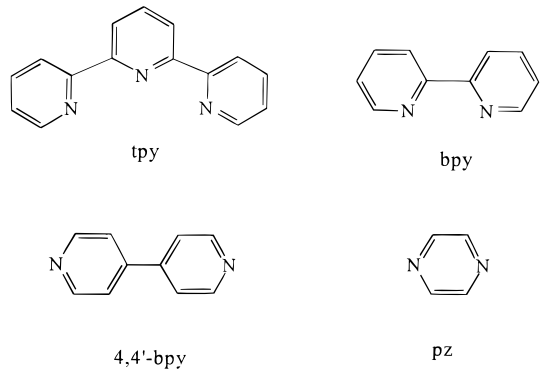

Figure 1. Ligand structures.

Measurements. UV−visible spectra were recorded on either a Bausch and Lomb 2000 or a Hewlett-Packard model 8451A diode array spectrophotometer. Near-infrared spectra were recorded on a Cary model 17I spectrophotometer by employing a data acquisition system with a Commodore Pet 4032 microcomputer and programs developed by Dr. Robert A. Binstead on a Cary model 14 spectrophotometer by using 2 mm path length quartz cells. Cyclic voltammetry was performed by using a Princeton Applied Research model 173 potentiostat and a model 175 universal programmer, a Pt bead working electrode, a Pt wire auxiliary electrode, and a saturated calomel reference electrode (SSCE). Infrared spectra were recorded on a Nicolet model 20DX Fourier transform infrared spectrometer by using a cell with CaF_2 windows and 1.35 mm path length.

Preparations. $Os^{IV}(bpy)Cl_4$,[11] *cis*-$Os^{II}(bpy)_2(Cl)_2$,[12] *cis*-$[Os(bpy)_2(Cl)(pz)](PF_6)_2$,[13] and *cis*-$[Os(bpy)_2(Cl)(4,4'\text{-}bpy)](PF_6)_2$[13] were synthesized according to published procedures.

$[(bpy)_2(Cl)Os(4,4'\text{-}bpy)Os(Cl)(bpy)_2](PF_6)_2$ ($\mathbf{1}^{2+}$). To 40 mL of 1:1 EtOH/H_2O were added 173 mg of $[Os(bpy)_2(Cl)(4,4'\text{-}bpy)](PF_6)$ (0.2 mM) and 94 mg of $Os(bpy)_2(Cl)_2$ (0.2 mM). The solution was stirred magnetically and heated at reflux for 2 days. The brown-purple complex was isolated as the PF_6^-

(7) (a) Creutz, C.; Taube, H. *J. Am. Chem. Soc.* **1969**, *91*, 3988. (b) Creutz, C.; Taube, H. *J. Am. Chem. Soc.* **1973**, *95*, 1086. (c) Richardson, D. E.; Taube, H. *Coord. Chem. Rev.* **1984**, *60*, 107. (d) Beattie, J. K.; Hush, N. S.; Taylor P. R. *Inorg. Chem.* **1976**, *15*, 992. (e) Tanner, M.; Ludi, A. *Chimia* **1980**, *34*, 23. (f) Hupp, J. T. *Proceedings of the 19th DOE Solar Photochemistry Research Conference*; DOE: Washington, DC, 1995; p 9. (g) Reid, P. J.; Silva, C.; Dong, Y.; Hupp, J. T.; Barbara, P. F. *Springer Ser. Chem. Phys.* **1994**, 505. (h) Krausz, E. *Chem. Phys. Lett.* **1985**, *120*, 113. (i) Krausz, E.; Ludi, A. *Inorg. Chem.* **1985**, *24*, 939.

(8) (a) Neyhart, G. A.; Hupp, J. T.; Curtis, J. C.; Timpson, C. J.; Meyer, T. J. *J. Am. Chem. Soc.* **1996**, *118*, 3724. (b) Neyhart, G. A.; Timpson, C. J.; Bates, W. D.; Meyer, T. J. *J. Am. Chem. Soc.* **1996**, *118*, 3730.

(9) (a) Demadis, K. D.; Meyer, T. J.; White, P. S. *Inorg. Chem.* **1997**, *36*, 5678. (b) Demadis, K. D.; El-Samanody, E.-S.; Coia, G. M.; Meyer, T. J. *J. Am. Chem. Soc.* **1999**, *121*, 535.

(10) Demadis, K. D.; Neyhart, G. A.; Kober, E. M.; Meyer, T. J. *J. Am. Chem. Soc.* **1998**, *120*, 7121.

(11) Buckingham, D. A.; Dwyer, F. P.; Sargeson, A. M. *Aust. J. Chem.* **1964**, *17*, 622.

(12) (a) Buckingham, D. A.; Dwyer, F. P.; Goodwin, H. A.; Sargeson, A. M. *Aust. J. Chem.* **1964**, *17*, 325. (b) Kober, E. M.; Caspar, J. V.; Sullivan, B. P.; Meyer, T. J. *Inorg. Chem.* **1988**, *27*, 4587.

(13) Kober, E. M. Ph.D. Dissertation, The University of North Carolina, Chapel Hill, NC, 1982.

salt and purified by chromatography (see Materials). Anal. Calcd for $Os_2Cl_2P_2F_{12}C_{60}H_{40}N_{10}\cdot 2H_2O$: C, 38.51; H, 2.82; N, 8.99. Found: C, 38.39; H, 2.28; N, 8.91.

$[(bpy)_2(Cl)Os(pz)Os(Cl)(bpy)_2](PF_6)_2$ (2^{2+}). To 40 mL of 1:1 EtOH/H_2O were added 154 mg of $[Os(bpy)_2(Cl)(pz)](PF_6)$ (0.2 mM) and 94 mg of $Os(bpy)_2(Cl)_2$ (0.2 mM). The solution was stirred magnetically and heated at reflux for 2 days. The deep violet complex was isolated as the PF_6^- salt and purified by chromatography (see Materials). Anal. Calcd for $Os_2Cl_2P_2F_{12}C_{44}H_{36}N_{10}$: C, 36.55; H, 2.51; N, 9.69. Found: C, 36.57; H, 2.42; N, 9.60.

Note: The oxidized forms $[(bpy)_2(Cl)Os(BL)Os(Cl)(bpy)_2]^{4+}$ (1^{4+} and 2^{4+}) were prepared as follows. To 30 mL of a 1:1 CH_3CN/H_2O solution were added 50 mg of 1^{2+} or 2^{2+} and excess NH_4PF_6. Sufficient $(NH_4)_2[Ce(NO_3)_6]$ was added with stirring until the color changed to yellow-orange and no further color change was noted. CH_3CN was removed in vacuo, resulting in the precipitation of the PF_6^- salts of 1^{4+} and 2^{4+}. The products were isolated by filtration, washed first with H_2O acidified with HPF_6 and then with Et_2O, and finally air-dried. Yields were almost quantitative, and the salts were assumed to be pure.

1^{3+} was prepared as follows. Equimolar amounts of 1^{2+} and oxidized 1^{4+} were dissolved in CH_3CN. The solution was stirred for several minutes and added dropwise to a 10-fold excess of Et_2O, resulting in the precipitation of 1^{3+} as its PF_6^- salt. 2^{3+} was prepared in the same manner. Yields were quantitative, and the salts were assumed to be pure.

$[Os(tpy)(bpy)(Cl)](PF_6)$. The preparation of the chloride salt of this complex was first reported by Buckingham et al.[11] Here we report a modified procedure for the PF_6^- salt. $Os(bpy)Cl_4$ (1.00 g, 2.04 mmol), tpy (0.54 g, 2.33 mmol), and ethylene glycol (50 mL) were combined in a 300 mL round-bottom flask. The mixture was heated at reflux under argon with magnetic stirring for 1 h. The solution was cooled to room temperature, followed by addition of 50 mL of H_2O and 5 mL of concentrated $Na_2S_2O_4$(aq). After 20 min of stirring at room temperature, the crude material was isolated as the black PF_6^- salt by addition of ~4 mL of saturated NH_4PF_6(aq). The precipitate was collected by filtration and dried in vacuo overnight. The crude material was purified by chromatography (see Materials) on a 6 in. × $1^1/_2$ in. alumina column packed in 1:1 CH_3CN/toluene. The moderately soluble salt was dissolved in the solvent mixture, and the solution was loaded onto the column with a pipet. Upon elution with the solvent mixture, the major product separated first as a purple-brown band. This band was collected and taken to dryness by rotary evaporation. The solid was reprecipitated by dissolving it in a minimum amount of CH_3CN and adding this solution dropwise to 500 mL of stirring Et_2O. The product was collected by filtration and dried in vacuo (yield: 55%).

$[Os(tpy)(bpy)(TFMS)](TFMS)_2$. A modification of the procedure of Takeuchi et al.[14] was used to isolate the triflate complex. A 0.20 g sample of $[Os(tpy)(bpy)(Cl)](PF_6)$ was added to a 25 mL round-bottom flask, and the flask was deaerated with argon. A 3 mL quantity of neat trifluoromethanesulfonic acid (triflic acid) was added, and the mixture was heated at reflux under argon with magnetic stirring for 1 h. The solution was cooled to room temperature and added dropwise to 500 mL of rapidly stirring anhydrous diethyl ether. The fluffy pale brown precipitate was collected by filtration and washed with an additional 250 mL of anhydrous Et_2O, minimizing any contact of the hygroscopic solid with air. The solid was immediately placed in a vacuum desiccator and stored in vacuo. The yield was assumed to be quantitative.

$[Os(tpy)(bpy)(4,4'\text{-}bpy)](PF_6)_2$. A sample of 4,4′-bpy (0.65 g) was dissolved in 5 mL of ethylene glycol, and the solution was degassed with argon. A 0.2 g amount of $[Os(tpy)(bpy)(TFMS)](TFMS)_2$ was rapidly added, and the solution was heated at reflux under argon with magnetic stirring for 15 min. After the reaction mixture was cooled to room temperature, 20 mL of H_2O was added, and the crude complex was isolated by addition of 2 mL of saturated NH_4PF_6(aq), collected by filtration, and washed with 5 mL of H_2O and 25 mL of Et_2O. The complex was further purified by chromatography on a 2.5 cm × 12 cm alumina column packed in 1:2 CH_3CN/toluene. The brown solid was dissolved in a minimum amount of the solvent mixture, and the solution was loaded onto the column with a pipet. Elution with the solvent mixture gave a brown band of the complex preceded by a lavender band and followed by a purple-brown band. The lavender band was discarded, and the brown band was collected by gradual enrichment of the eluant to 1:1 CH_3CN/toluene. The complex was taken to dryness by rotary evaporation and reprecipitated by dissolving it in a minimum amount of CH_3CN and adding the solution dropwise to 150 mL of Et_2O under stirring. Yield: 140 mg (53%). Anal. Calcd for $OsP_2F_{12}C_{35}H_{27}N_7\cdot H_2O$: C, 40.27; H, 2.71; N, 9.39. Found: C, 40.36; H, 2.76; N, 9.43.

Note: Os^{III} in $[Os(tpy)(bpy)(TFMS)](TFMS)_2$ is reduced to Os^{II} by the solvent during the reaction. The primary Os^{II} impurity appeared to be $[Os^{II}(tpy)(bpy)(OH_2)]^{2+}$.[14] H_2O is introduced either from the "wet" solvent or from the atmosphere during the handling of the hygroscopic TFMS salt. $[Os^{II}(tpy)(bpy)(OH_2)]^{2+}$ is substitutionally inert. It does not react with 4,4′-bpy (in 20-fold excess) in a 1:1 EtOH/H_2O mixture under reflux. *The interference of water in the preparations appeared to be more severe for the pz-bridged complexes.*

$[Os(tpy)(bpy)(pz)](PF_6)_2$ was prepared in the same manner but using an equivalent excess of pz.

$[(tpy)(bpy)Os(4,4'\text{-}bpy)Os(bpy)(tpy)](PF_6)_4$ (3^{4+}). This salt was prepared by the reaction between $[Os(tpy)(bpy)(4,4'\text{-}bpy)]^{2+}$ and $[Os(tpy)(bpy)(TFMS)]^{2+}$. In a typical preparation, $[Os(tpy)(bpy)(4,4'\text{-}bpy)](PF_6)_2$ (0.10 g, 0.097 mmol) and 5 mL of ethylene glycol were added to a 50 mL round-bottom flask and the mixture was degassed with argon. $[Os(tpy)(bpy)(TFMS)](TFMS)_2$ (0.095 g, 0.097 mmol) was rapidly weighed out and added to the reaction mixture. The solution was heated at reflux under argon with magnetic stirring for 2 h. The mixture was cooled to room temperature, and the crude dimer was isolated by the addition of 40 mL of H_2O and 3 mL of saturated NH_4PF_6(aq). The dark brown precipitate was collected by filtration and dried overnight in vacuo. The crude material was purified by chromatography on a 4 in. × $^3/_4$ in. alumina column packed in 1:1 CH_3CN/toluene. The solid was dissolved in a minimum of the solvent mixture and loaded onto the column with a pipet. Upon elution with the solvent mixture, the dark brown band of the dimer was eluted after a reddish brown band and a pale brown band. After removal of the first two bands, the desired product was eluted by changing the eluant to neat CH_3CN. The dark brown band was collected and taken to dryness by rotary evaporation. The pure dimer was reprecipitated by dissolving it in a minimum amount of CH_3CN and adding the solution to 150 mL of stirring Et_2O. Yield: 40%. Anal. Calcd for $Os_2P_4F_{24}C_{60}H_{44}N_{12}\cdot 2H_2O$: C, 37.31; H, 2.61; N, 8.70. Found: C, 37.44; H, 2.72; N, 8.71.

$[(tpy)(bpy)Os^{II}(pz)Os^{II}(bpy)(tpy)](PF_6)_4$ (4^{4+}) was prepared and isolated in the same manner as described for 3^{4+} by reacting

(14) Takeuchi, K. J.; Thomson, M. S.; Pipes, D. W.; Meyer, T. J. *Inorg. Chem.* **1984**, *23*, 1845.

Table 1. Summary of Crystal Data and Intensity Collection and Structure Refinement Parameters for $[(tpy)(bpy)Os^{II}(4,4'\text{-bpy})OS^{II}(bpy)(tpy)](PF_6)_4\cdot 2CH_3CN$ ($\mathbf{3}^{4+}$)

salt	3^{4+}	collection temp (°C)	−100
formula	$Os_2C_{64}H_{52}P_4F_{24}N_{14}$	abs coeff, μ (cm^{-1})	3.80
mol wt	1977.45	$F(000)$	1922.91
a (Å)	12.0227(8)	$2\theta_{max}$ (deg)	50.0
b (Å)	15.0695(11)	no. of total reflns	19 048
c (Å)	19.5000(14)	no. of unique reflns	6241
β (deg)	92.959(1)	no. of refined reflns	4455
V ($Å^3$)	3528.2(4)	merging R value	0.042
Z	2	no. of parameters	487
crystal system	monoclinic	R (%)[a]	3.8
space group	$P2_1/c$	R_w (%)[b]	4.6
crystal size (mm)	0.20 × 0.15 × 0.05	goodness of fit[c]	2.75
d_{calcd} (g/cm^3)	1.861	deepest hole ($e/Å^3$)	−1.010
diffractometer	Siemens CCD Smart	highest peak ($e/Å^3$)	1.250
radiation (λ (Å))	Mo Kα (0.710 73)		

[a] $R = \sum(|F_o - F_c|)/\sum|F_o|$. [b] $R_w = [\sum(w|F_o - F_c|^2/\sum(wF_o^2)]^{1/2}$. [c] GoF $= [\sum w(F_o - F^c)^2/(\text{no. of reflections} - \text{no. of parameters})]^{1/2}$.

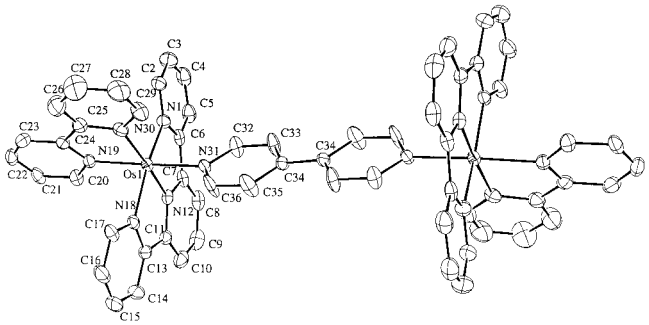

Figure 2. ORTEP diagram (30% probability ellipsoids) of the cation $\mathbf{3}^{4+}$ in the salt $[(tpy)(bpy)Os(4,4'\text{-bpy})Os(bpy)(tpy)](PF_6)_4$.

equimolar amounts of $[Os(tpy)(bpy)(pz)](PF_6)_2$ and $[Os(tpy)(bpy)(TFMS)](TFMS)_2$.

$[(tpy)(bpy)Os(4,4'\text{-bpy})Os(bpy)(tpy)](PF_6)_5$ ($\mathbf{3}^{5+}$) was prepared by $(NH_4)_2[Ce(NO_3)_6]$ oxidation of $\mathbf{3}^{4+}$ in 1:1 CH_3CN/H_2O followed by removal of CH_3CN and precipitation of $\mathbf{3}^{6+}$ in the same manner as described for dimers $\mathbf{1}^{4+}$ and $\mathbf{2}^{4+}$. $\mathbf{3}^{5+}$ was generated in solution by combining equimolar amounts of $\mathbf{3}^{4+}$ and $\mathbf{3}^{6+}$.

$[(tpy)(bpy)Os(pz)Os(bpy)(tpy)]^{6+}$ ($\mathbf{4}^{5+}$). The fully oxidized $Os^{III}-Os^{III}$ form of this dimer was not stable either in solution or in the solid state. The mixed-valence form of the pz-bridged dimer was generated in situ just prior to use by careful addition of $(NH_4)_2[Ce^{IV}(NO_3)_6]$ in CH_3CN. Overoxidation occasionally resulted in formation of a purple precipitate, presumably the NO_3^- salt.

X-ray Structure Determination: Data Collection and Solution and Refinement of the Structure. Single crystals of $\mathbf{3}^{4+}$ as the PF_6^- salt were obtained by slow diffusion of Et_2O into a CH_3CN solution of $\mathbf{3}^{5+}$. During the crystallization process, crystals of $\mathbf{3}^{4+}$ (nearly black rectangular plates) and crystals of $\mathbf{3}^{6+}$ (yellow-green needles, nondiffracting) were isolated. Crystal data, intensity collection information, and structure refinement parameters for the structure are provided in Table 1. The structure was solved by direct methods. The remaining nonhydrogen atoms were located in subsequent difference Fourier maps. Empirical absorption corrections were applied with SADABS. The ORTEP plotting program was used to computer-generate the structure shown in Figure 2.[15] Hydrogen atoms were included in calculated positions with thermal parameters derived from the atoms to which they were bonded. All computations were performed by using the NRCVAX suite of programs.[16] Atomic scattering factors were taken from a standard source[17] and corrected for anomalous dispersion.

The crystal of $\mathbf{3}^{4+}$ contains two CH_3CN molecules per asymmetric unit. The final positional parameters, along with their standard deviations as estimates from the inverse matrix, and anisotropic thermal parameters are available as Supporting Information. Bond lengths and angles in $\mathbf{3}^{4+}$ are given in Table 2. They use the numbering scheme in Figure 2.

Table 2. Selected Bond Distances (Å) and Angles (deg) in $\mathbf{3}^{4+}$ with Labeling According to Figure 2

Bonds			
Os(1)−N(1)	2.077(6)	N(31)−C(36)	1.329(12)
Os(1)−N(12)	1.961(7)	C(32)−C(33)	1.363(14)
Os(1)−N(18)	2.062(7)	C(33)−C(34)	1.373(13)
Os(1)−N(19)	2.065(7)	C(34)−C(34a)	1.467(15)
Os(1)−N(30)	2.084(7)	C(34)−C(35)	1.388(14)
Os(1)−N(31)	2.115(6)	C(35)−C(36)	1.369(16)

Angles			
N(1)−Os(1)−N(12)	79.9(3)	N(1)−Os(1)−N(18)	158.6(3)
N(1)−Os(1)−N(19)	91.3(3)	N(1)−Os(1)−N(30)	100.8(3)
N(1)−Os(1)−N(31)	93.3(3)	N(12)−Os(1)−N(18)	79.3(3)
N(12)−Os(1)−N(19)	99.0(3)	N(12)−Os(1)−N(30)	176.4(3)
N(12)−Os(1)−N(31)	89.3(3)	N(18)−Os(1)−N(19)	87.3(3)
N(18)−Os(1)−N(30)	99.7(3)	N(18)−Os(1)−N(31)	91.1(3)
N(19)−Os(1)−N(30)	77.5(3)	N(19)−Os(1)−N(31)	171.1(3)
N(30)−Os(1)−N(31)	94.2(3)		

Results

Molecular Structure of $[(tpy)(bpy)Os^{II}(4,4'\text{-bpy})Os^{II}(bpy)(tpy)](PF_6)_4\cdot 2CH_3CN$. In the structure of the PF_6^- salt of $\mathbf{3}^{4+}$ (Figure 2), 4,4′-bpy bridges the two Os centers. The Os−N(tpy) (1.961(7) Å, central; 2.077(6) and 2.062(7) Å, peripheral) and Os−N(bpy) (2.084(7), 2.065(7) Å) bond distances are unexceptional and consistent with Os^{II}.[18] The two pyridyl rings of μ-4,4′-bpy are coplanar. The Os−N(4,4′-bpy) bond is relatively long at 2.115(6) Å. The dihedral angle between the ring of 4,4′-bpy and the ring of the bpy in the trans position is ∼ 62°.

(15) Johnson, C. K. *ORTEP: A Fortran thermal ellipsoid plot program*; Technical Report ORNL-5138; Oak Ridge National Laboratory: Oak Ridge, TN, 1976.

(16) Gabe, E. J.; Le Page, Y.; Charland, J.-P.; Lee, F. L.; White, P. S. *J. Appl. Crystallogr.* **1989**, *22*, 384.

(17) *International Tables for X-ray Crystallography*; Kynoch Press: Birmingham, U.K., 1974; Vol. IV.

(18) $Os^{II}-N$ bond lengths: (a) Demadis, K. D.; Meyer, T. J.; White, P. S. *Inorg. Chem.* **1998**, *37*, 3610. (b) Constable, E. C.; Raithby, P. R.; Smit, D. N. *Polyhedron* **1989**, *8*, 367. (c) Richter, M. M.; Scott, B.; Brewer, K. J.; Willett, R. D. *Acta Crystallogr.* **1991**, *C47*, 2443. (d) Shklover, V.; Zakeeruddin, S. M.; Nesper, R.; Fraser, D.; Grätzel, M. *Inorg. Chim. Acta* **1998**, *274*, 64. (e) *Gmelins Handbuch der Anorganischen Chemie: Osmium, Supplement*; Springer-Verlag: Berlin, 1980; Vol. 1 and references therein.

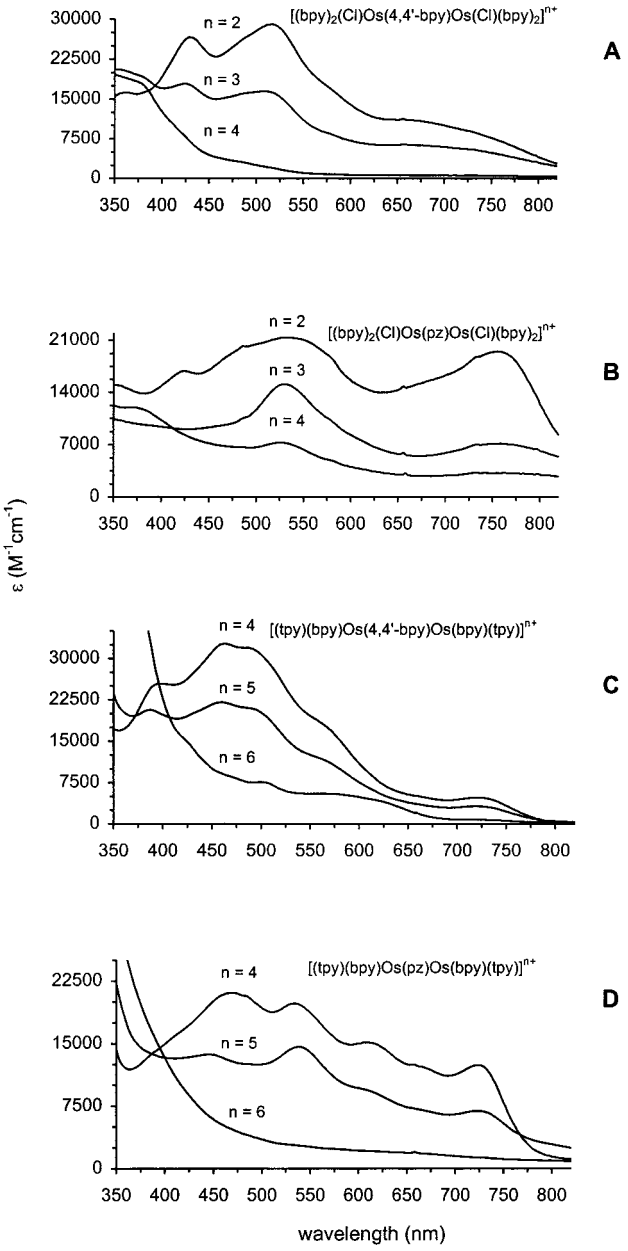

Figure 3. UV−visible spectra in CH_3CN.

UV−Visible Spectra. The low-energy spectra of the Os^{II} complexes in CH_3CN are dominated by $d\pi \rightarrow \pi^*$ metal-to-ligand charge-transfer (MLCT) bands. For Os^{III}, MLCT bands and $Cl^- \rightarrow Os^{III}$ charge-transfer bands of low absorptivity appear at higher energy.[13,19,20] Spectra of $[(bpy)_2(Cl)Os(BL)Os(Cl)(bpy)_2]^{n+}$ ($n = 2$, 3, 4; BL = pz, 4,4′-bpy) and $[(tpy)(bpy)Os(BL)Os(bpy)(tpy)]^{n+}$ ($n = 4$, 5, 6) are shown in Figure 3, with results summarized in Table 3.

The Os^{II} MLCT spectra consist of a series of overlapping bands of high absorptivity arising from transitions that give excited states that are largely singlet in character and, at lower energy and lower absorptivity, states that are largely triplet in character. The spin character of the excited states is highly mixed due to spin−orbit coupling. The spectrum of $\mathbf{1}^{2+}$ is roughly twice that of *cis*-$[Os(bpy)_2(Cl)(4,4'\text{-bpy})]^+$. From the electrochemical data (which show that initial reduction is at 4,4′-bpy), the low-energy spectrum arises from a convolution of $Os^{II}(d\pi) \rightarrow bpy(\pi^*)$, and $Os^{II}(d\pi) \rightarrow 4,4'\text{-bpy}(\pi^*)$ transitions. Similarly, the spectrum of $\mathbf{1}^{4+}$ is nearly twice that of *cis*-$[Os(bpy)_2(Cl)(py)]^{2+}$.[13] The spectrum of $\mathbf{1}^{3+}$ is essentially an average of those of $\mathbf{1}^{2+}$ and $\mathbf{1}^{4+}$.

In the spectrum of $\mathbf{2}^{2+}$, an intense $Os^{II}(d\pi) \rightarrow pz(\pi^*)$ band appears at 762 nm (13100 cm^{-1}), with a shoulder at 708 nm (14100 cm^{-1}). Intense bands appear at higher energy, including a band at 560 nm (17900 cm^{-1}). The bands at 762 and 560 nm are of nearly equal absorptivity, and there are no bands of lower absorptivity in the near-infrared. Normally, these low-energy bands are of relatively low absorptivity and can be assigned to the "triplet" analogue of "singlet" transitions at higher energy, as noted above.[13] The surprising absorptivity of the 760 nm band is apparently a consequence of extensive Os−Os coupling across the bridge resulting in even further mixing of the MLCT "singlet" and "triplet" excited states.

For $\mathbf{2}^{3+}$, an intense MLCT band appears at 540 nm (18520 cm^{-1}) and a $Os^{II}(d\pi) \rightarrow pz(\pi^*)$ band appears at 770 nm (∼13000 cm^{-1}). An additional band appears in the near-infrared at 1120 nm (8930 cm^{-1}). It is ∼4000 cm^{-1} to lower energy and may be the "triplet" analogue of $Os^{II}(d\pi) \rightarrow pz(\pi^*)$. The spectrum of $\mathbf{2}^{4+}$ is essentially twice the spectrum of $[Os^{III}(bpy)_2(pz)(Cl)]^{2+}$ [13] and presents no unusual features.

A series of intense, overlapping $Os^{II}(d\pi) \rightarrow pz(\pi^*)$, $Os^{II}(d\pi) \rightarrow bpy(\pi^*)$, and $Os^{II}(d\pi) \rightarrow tpy(\pi^*)$ bands are observed in the visible for $\mathbf{3}^{4+}$. The spectrum of $\mathbf{3}^{4+}$ is essentially twice the spectrum of $[Os^{II}(tpy)(bpy)(4,4'\text{-bpy})]^{2+}$. There is a rising absorption in the visible for $\mathbf{3}^{6+}$ with shoulders at ∼570, 520, and 450 nm. The spectrum of $\mathbf{3}^{5+}$ is essentially the sum of the spectra of $\mathbf{3}^{4+}$ and $\mathbf{3}^{6+}$, as shown in Figure 3C.

In the spectrum of $\mathbf{4}^{4+}$, there are a series of intense, overlapping bands in the visible at 724 nm (13810 cm^{-1}), 668 nm (14970 cm^{-1}), 616 nm (16230 cm^{-1}), 538 nm (18590 cm^{-1}), and 450 nm (22220 cm^{-1}), Figure 3D and Table 3. The band at 724 nm can be assigned to the $Os^{II}(d\pi) \rightarrow pz(\pi^*)$ transition to the lowest, largely triplet excited state, and the others to a combination of $Os^{II}(d\pi) \rightarrow bpy(\pi^*)$, $Os^{II}(d\pi) \rightarrow tpy(\pi^*)$, and $Os^{II}(d\pi) \rightarrow pz(\pi^*)$ transitions. The pattern of bands is similar to those for $\mathbf{3}^{4+}$ and $[Os^{II}(tpy)(bpy)(pz)]^{2+}$, but the low-energy bands are more intense (Table 3). The $\mathbf{4}^{6+}$ ion is essentially featureless in the visible with $\pi \rightarrow \pi^*$(bpy, tpy) bands appearing in the UV. The spectrum of $\mathbf{4}^{5+}$ is similar to that of $\mathbf{4}^{4+}$, but the bands are less intense and somewhat shifted. The spectrum of $\mathbf{4}^{5+}$ is nearly the sum of the spectra of $\mathbf{4}^{4+}$ and $\mathbf{4}^{6+}$, but there are significant differences in detail reflecting the influence of metal−metal electronic coupling across the bridge.

The complexity of the $Os^{II}(tpy)(bpy)(pz)$-based spectra is expected since there are separate π^* acceptor levels on the separate ligands and transitions to them from the $d\pi_1$, $d\pi_2$, and $d\pi_3$ levels at Os^{II}.

Electrochemistry. Electrochemical data obtained by cyclic voltammetry are summarized in Table 3. For $\mathbf{1}^{2+}$, a single, unresolved $Os^{III/II}$ wave appears at $E_{1/2} = +0.37$ V. The splitting between the oxidative and reductive peak current maxima is $\Delta E_p = 90$ mV, $n = 2$ by coulometry (oxidation at +0.7 V and rereduction at 0.0 V). These observations are consistent with closely spaced $Os^{III}-Os^{II}/Os^{II}-Os^{II}$ and $Os^{III}-Os^{III}/Os^{III}-Os^{II}$ waves in the cyclic voltammogram. The peak current for the reduction at $E_{1/2} = -1.25$ V is half that of the $Os^{III/II}$ wave at $E_{1/2} = 0.37$ V, consistent with one-electron reduction at 4,4′-bpy. Subsequent bpy-based reductions appear at $E_{1/2} > -1.5$ V.[21−23] For $\mathbf{2}^{2+}$, $Os^{III}-Os^{II}/Os^{II}-Os^{II}$ and $Os^{III}-Os^{III}/Os^{III}-Os^{II}$

(19) Kober, E. M.; Meyer, T. J. *Inorg. Chem.* **1983**, *22*, 1614.
(20) Kober, E. M.; Meyer, T. J. *Inorg. Chem.* **1982**, *21*, 3967.
(21) Sullivan, B. P.; Caspar, J. V.; Johnson, S. R.; Meyer, T. J. *Organometallics* **1984**, *3*, 1241.

Table 3. UV−Visible and Electrochemical Data in CH_3CN vs SSCE, in 0.1 M TBAH for $E_{1/2}$ Values

complex	λ_{max} (nm) (ϵ (M^{-1} cm^{-1}))	$E_{1/2}$ (V) oxidations	$E_{1/2}$ (V) reductions
$[Os^{II}(tpy)(bpy)(4,4'\text{-bpy})]^{2+}$	723 (1800), 458 (12 500), 373, (12 000), 317 (37 800), 290 (36 600), 246 (32 800)	+0.88 ($Os^{III/II}$)	−1.17 ($bpy^{0/-}$) −1.51 ($bpy^{2-/-}$)
$[Os^{II}(tpy)(bpy)(pz)]^{2+}$	706 (2200), 536 (sh, 5600), 470 (12 900), 458 (13 300), 372 (12 000), 316 (44 900), 288 (42 400)	+0.94 ($Os^{III/II}$)	−1.13 ($bpy^{2-/-}$) −1.45 ($bpy^{0/-}$)
$[Os^{II}(bpy)_2(Cl)(pz)]^{+}$	710 (sh), 650 (2800), 501 (11 000), 470 (sh), 350 (sh), 295 (49 000), 255 (sh), 245 (20 500)	+0.43 ($Os^{III/II}$) +1.88 ($Os^{IV/III}$)	−1.40 ($bpy^{0/-}$) −1.64 ($bpy^{2-/-}$)
$[Os^{II}(bpy)_2(Cl)(4,4'\text{-bpy})]^{+}$	740 (sh), 660 (2950), 515 (15 200), 480 (sh), 410 (15 200), 360 (sh), 296 (59 000), 291 (sh), 253 (sh), 245 (39 000)	+0.38 ($Os^{III/II}$) +1.83 ($Os^{IV/III}$)	−1.43 ($bpy^{0/-}$) −1.66 ($bpy^{2-/-}$)
$[(bpy)_2(Cl)Os^{II}(4,4'\text{-bpy})Os^{II}(Cl)(bpy)_2]^{2+}$ (**1**$^{2+}$)	710 (broad, ∼11 000), 518 (29 000), 426 (27 500), 364 (15 000), 315 (sh, ∼65 000), 296 (150 000), 246 (110 000)	+0.37 ($Os^{III/III}-Os^{III/II}$ + $Os^{III/II}-Os^{II/II}$)	−1.25 ($4,4'\text{-bpy}^{0/-}$) ∼−1.50 ($bpy^{0/-}$) ∼−1.53 ($bpy^{2-/-}$)
$[(bpy)_2(Cl)Os^{III}(4,4'\text{-bpy})Os^{III}(Cl)(bpy)_2]^{4+}$ (**1**$^{4+}$)	540 (2000), 360 (sh, ∼19 000), 310 (62 000), 295 (140 000), 245 (120 000)		
$[(bpy)_2(Cl)Os(4,4'\text{-bpy})Os(Cl)(bpy)_2]^{3+}$ (**1**$^{3+}$)	710 (broad, ∼6000), 518 (16 000), 425 (16 000), 360 (15 000), 315 (sh, ∼65 000), 296 (150 000), 246 (110 000)		
$[(bpy)_2(Cl)Os^{II}(pz)Os^{II}(Cl)(bpy)_2]^{2+}$ (**2**$^{2+}$)	762 (19 500), 708 (sh, ∼15 000), 534 (22 000), 492 (20 500), 428 (15 500), 356 (13 000), 315 (78 000), 290 (85 000)	+0.42 ($Os^{III/II}-Os^{II/II}$)	−1.17 ($pz^{0/-}$) −1.55 ($bpy^{2-/-}$ + $bpy^{0/-}$, unresolved)
$[bpy)_2(Cl)Os^{III}(pz)Os^{III}(Cl)(bpy)_2]^{4+}$ (**2**$^{4+}$)	a rising absorption from 800 to 450 nm, 370 (sh, ∼12 000), 313 (80 000), 290 (84 500)		
$[(bpy)_2(Cl)Os(pz)Os(Cl)(bpy)_2]^{3+}$ (**2**$^{3+}$)	764 (7000), 532 (17 500), 430 (8500), 358 (9000), 315 (81 000), 290 (85 000)		
$[(tpy)(bpy)Os^{II}(4,4'\text{-bpy})Os^{II}(bpy)(tpy)]^{4+}$ (**3**$^{4+}$)	720 (4900), 560 (17 500), 461 (32 700), 396 (25 500), 317 (90 300), 290 (89 800), 243 (81 000)	+0.87 ($Os^{III/III}-Os^{III/II}$ + $Os^{III/II}-Os^{II/II}$)	−1.15 ($bpy^{0/-}$) −1.53 ($bpy^{2-/-}$)
$[(tpy)(bpy)Os^{III}(4,4'\text{-bpy})Os^{III}(bpy)(tpy)]^{6+}$ (**3**$^{6+}$)	720 (∼1000), ∼600 (broad, 5000), 505 (7500), 425 (sh, 14 000), 315 (9000), 290 (90 000), 242 (sh, ∼80 000)		
$[(tpy)(bpy)Os(4,4'\text{-bpy})Os(bpy)(tpy)]^{5+}$ (**3**$^{5+}$)	720 (2500), 5600 (11 000), 460 (22 000), 396 (20 000), 317 (63 000), 290 (69 000), 220 (60 000)		
$[(tpy)(bpy)^{II}Os(pz)Os^{II}(bpy)(tpy)]^{4+}$ (**4**$^{4+}$)	721 (12 400), 609 (15 100), 533 (20 000), 468 (21 000), 315 (62 300), 287 (68 600), 222 (60 000)	+1.12 ($Os^{III/III}-Os^{III/II}$) +0.96 ($Os^{III/II}-Os^{II/II}$)	−0.80 ($pz^{0/-}$) −1.13 ($bpy^{0/-}$) −1.21 ($bpy^{2-/-}$)
$[(tpy)(bpy)^{III}Os(pz)Os^{III}(bpy)(tpy)]^{6+}$ (**4**$^{6+}$)	a rising absorption from 800 to 450 nm, 344 (63 000), 320 (70 000), 285 (69 000), 220 (71 000)		
$[(tpy)(bpy)Os(pz)Os(bpy)(tpy)]^{5+}$ (**4**$^{5+}$)	724 (7000), 668 (6900), 616 (9500), 538 (15 000), 450 (14 000), 313 (63 300), 290 (68 300), 220 (61 000)		

waves appear at +0.42 and +0.61 V ($\Delta E_{1/2}$ = 190 mV). Oxidative coulometry of **2**$^{2+}$ at +1.0 V and subsequent reduction at 0.0 V occur with n = 2, indicating that both couples are one-electron processes and chemically reversible. One-electron reduction occurs at pz at $E_{1/2}$ = −1.17 V. It is followed by a two-electron reduction at $E_{1/2}$ = −1.55 V, which is the overlap of two one-electron bpy-centered reductions.

Related observations are made in comparing the electrochemical properties of $[(tpy)(bpy)Os(BL)Os(bpy)(tpy)]^{4+}$ with BL = 4,4′-bpy (**3**$^{4+}$) and pz (**4**$^{4+}$). For **4**$^{4+}$, $Os^{III}-Os^{II}/Os^{II}-Os^{II}$ and $Os^{III}-Os^{III}/Os^{III}-Os^{II}$ waves appear at +0.96 and +1.12 V ($\Delta E_{1/2}$ = 160 mV). For **3**$^{4+}$, a single two-electron wave is observed at +0.87 V. In both cases, the first oxidation is approximately at the same potential as oxidation of the corresponding monomer. Reductively, waves corresponding to tpy or 2,2′-bpy ring reductions [24,25] are observed at −1.15 and −1.53 V for **3**$^{4+}$ and at −1.13 and −1.21 V for **4**$^{4+}$. For **3**$^{4+}$, waves at similar potentials are observed, but a new wave at −0.95 V from 4,4′-bpy reduction also appears. In **4**$^{4+}$, pz-based reduction occurs at −0.80 V.

Infrared Spectra. Spectra for the series of dimers in CD_3CN were acquired in the ν(bpy), ν(tpy) ring-stretching region from 1300 to 1650 cm^{-1}. In Figure 4A are shown spectra of **1**$^{2+}$, **1**$^{4+}$, and **1**$^{3+}$ compared to a spectrum constructed from the sum of **1**$^{2+}$ and **1**$^{4+}$. The same set of spectra is shown in Figure 4B−D for **2**$^{2+}$, **2**$^{3+}$ and **2**$^{4+}$; **3**$^{4+}$, **3**$^{5+}$ and **3**$^{6+}$; and **4**$^{4+}$, **4**$^{5+}$ and **4**$^{6+}$. Band energies are listed in a table in the Supporting Information.

For the 4,4′-bpy mixed-valence complexes (**1**$^{3+}$ and **3**$^{5+}$), the observed and average spectra in Figure 4A,C are essentially superimposable. For **2**$^{3+}$, ν(bpy) bands at 1316, 1423, 1450, 1465, and 1487 cm^{-1} are the average of bands at 1312/1319, 1421/1426, 1447/1451, and 1461/1469 cm^{-1} (**2**$^{2+}$/**2**$^{4+}$). In KBr, the energies of these bands are as follows (**2**$^{2+}$, **2**$^{3+}$, **2**$^{4+}$): 1420, 1421, 1426; 1447, 1448, 1450; 1460, 1459, 1468; 1478, 1475, 1485 cm^{-1}. On the basis of Kincaid's normal-coordinate analysis for $[Ru^{II}(bpy)_3]^{2+}$,[27b,c] the ν(bpy) band assignments and local mode contributions are as follows: 1487 cm^{-1} (ν_{18}; 25% ν(Os−N), 16% $\nu(C_1-C_1')$, 12% ν(CCC), 11% ν(C−N)) + ν_{33}; 35% δ(CCH), 13% (C_2-C_3), 11% α(CCC)); 1467 cm^{-1} (ν_{27}; 35% $\delta(C_1C_2H)$, 25% δ(CCH), 21% $\nu(C_3-C_4)$, 14% (ν(C−N)); 1451 cm^{-1} (ν_{18} + γ(CH); 25% ν(Os−N), 16% α(CCC), 11%

(22) Root, M. J.; Sullivan, B. P.; Meyer, T. J.; Deutsch, E. *Inorg. Chem.* **1985**, *24*, 2731.
(23) Roffia, S.; Ciano, M. *J. Electroanal. Chem. Interfacial Electrochem.* **1979**, *100*, 809.
(24) Seok, W. K.; Dobson, J. C.; Meyer, T. J. *Inorg. Chem.* **1988**, *27*, 3.
(25) Pipes, D. W.; Meyer, T. J. *Inorg. Chem.* **1986**, *25*, 4042.
(26) Powers, M. J.; Meyer, T. J. *Inorg. Chem.* **1978**, *17*, 1785.
(27) (a) Omberg, K. M.; Schoonover, J. R.; Treadway, J. A.; Leasure, R. M.; Dyer, R. B.; Meyer, T. J. *J. Am. Chem. Soc.* **1997**, *119*, 7013. (b) Mallick, P. K.; Danzer, G. D.; Strommen, D. P.; Kincaid, J. R. *J. Phys. Chem.* **1988**, *92*, 5628. (c) Strommen, D. P.; Mallick, P. K.; Danzer, G. D.; Lumpkin, R. S.; Kincaid, J. R. *J. Phys. Chem.* **1990**, *94*, 1357.

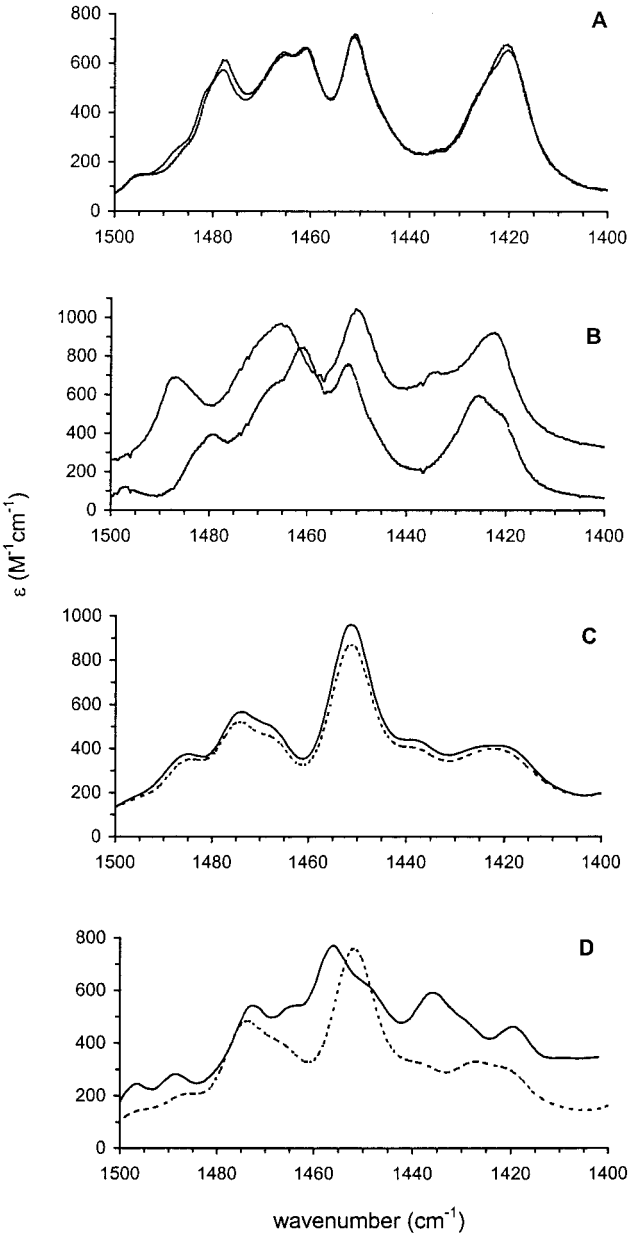

Figure 4. Infrared spectra of $[(bpy)_2(Cl)Os(BL)Os(Cl)(bpy)_2]^{3+}$ (BL = 4,4′-bpy(A); BL = pz (B) and of $[(tpy)(bpy)Os(BL)Os(bpy)(tpy)]^{5+}$ (BL = 4,4′-bpy, (C); BL = pz (D)) from 1400 to 1500 cm^{-1} in CD_3CN:—, experimental; - - - calculated. The calculated spectra are one-half the sum of the spectra of the ions $\mathbf{1}^{2+}$ and $\mathbf{1}^{4+}$ (A), $\mathbf{2}^{2+}$ and $\mathbf{2}^{4+}$ (B), $\mathbf{3}^{4+}$ and $\mathbf{3}^{6+}$ (C), and $\mathbf{4}^{4+}$ and $\mathbf{4}^{6+}$ (D).

ν(C−N)); 1429 cm^{-1} (ν_{28}; 47% δ(CCH), 28% $\nu(C_1-C_2)$, 14% $\delta(C_1C_2H)$).[27a]

The spectrum of $\mathbf{4}^{5+}$ is complex due to the presence of both ν(bpy) and ν(tpy) bands. There is a total of 10 bands in the 1300−1500 cm^{-1} region (see Figure 4D). Comparison of the bands for $\mathbf{4}^{4+}$, $\mathbf{4}^{5+}$, and $\mathbf{4}^{6+}$ reveals a complicated band pattern that is not half the sum of $\mathbf{4}^{4+}$ and $\mathbf{4}^{6+}$ bands. The band for $\mathbf{4}^{5+}$ at 1489 cm^{-1} may be the average of 1486 cm^{-1} for $\mathbf{4}^{4+}$ and 1495 cm^{-1} for $\mathbf{4}^{6+}$. The band at 1473 cm^{-1} for $\mathbf{4}^{5+}$ may be an average of bands at 1465 cm^{-1} for $\mathbf{4}^{4+}$ and 1475 cm^{-1} for $\mathbf{4}^{6+}$. The remaining bands in the 1440−1470 cm^{-1} region correspond neither to half the sum of $\mathbf{4}^{4+}$ and $\mathbf{4}^{6+}$ bands nor to the average of bands for $\mathbf{4}^{4+}$ and $\mathbf{4}^{6+}$. The observed band pattern is too complex to describe by a simple model.

ν(pz) appears at 1599 cm^{-1} (ϵ = 2600 M^{-1} cm^{-1}) for $\mathbf{2}^{3+}$ and at 1594 cm^{-1} (ϵ = 2020 M^{-1} cm^{-1}) for $\mathbf{4}^{5+}$. This band is absent in the spectra of $\mathbf{2}^{2+}$, $\mathbf{2}^{4+}$, $\mathbf{4}^{4+}$, and $\mathbf{4}^{6+}$. For comparison, ν(pz) in the spectrum of *cis*-$[Os^{II}(bpy)_2(Cl)(pz)]^+$ appears at 1584 cm^{-1} (ϵ = 600 M^{-1} cm^{-1}).[10]

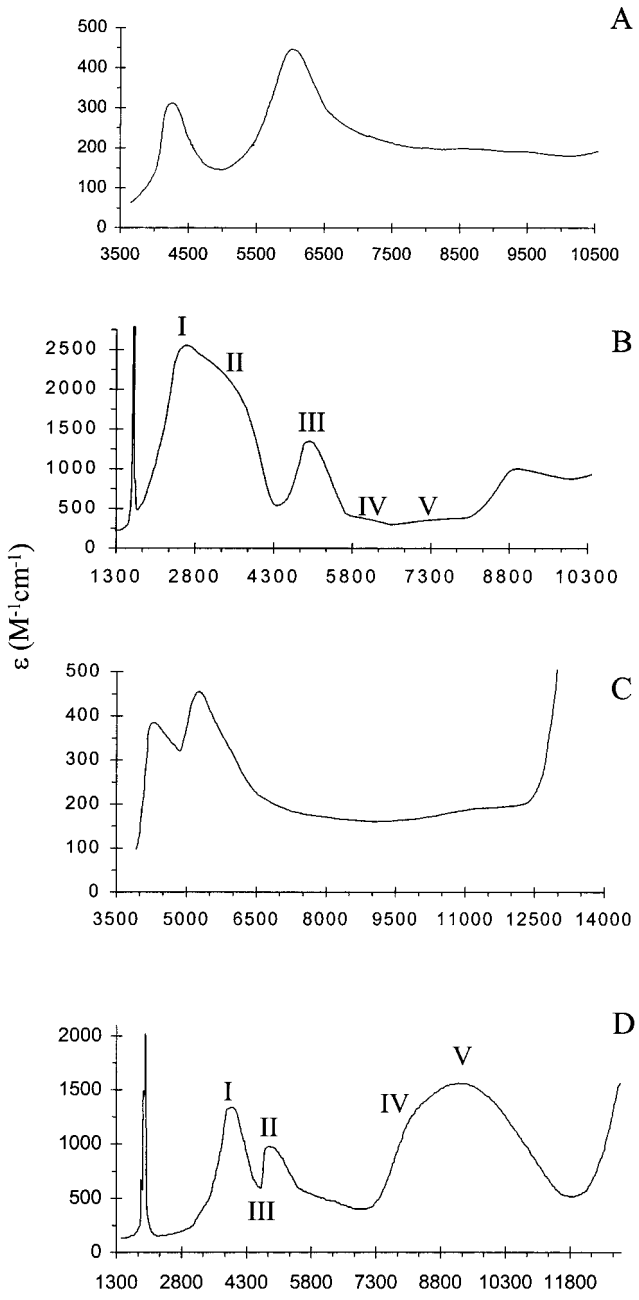

Figure 5. Near-infrared spectra of the mixed-valence ions $\mathbf{1}^{3+}$ (A), $\mathbf{2}^{3+}$ (B), $\mathbf{3}^{5+}$ (C), and $\mathbf{4}^{5+}$ (D) in CD_3CN. Solvent overtone bands are not shown.

Near-Infrared Spectra in CD_3CN. Near-infrared spectra are shown in Figure 5. Spectra plotted as $\int\epsilon(\bar{\nu})\,d\bar{\nu}/\bar{\nu}$ vs $\bar{\nu}$ are shown in Figure S1 in the Supporting Information. The NIR spectra of $\mathbf{2}^{3+}$ and $\mathbf{4}^{5+}$ were scaled as $\int\epsilon(\bar{\nu})\,d\bar{\nu}/\bar{\nu}$ and deconvoluted by use of the software package GRAMS 32. Band maxima (E_{abs}), molar extinction coefficients (ϵ), and bandwidths ($\Delta\bar{\nu}_{1/2}$) were derived from the deconvolution procedure and are given in Table 4. After spectral deconvolution, bands appear at 2620, 3590, 4960, 6000, and 7500 cm^{-1} for $\mathbf{2}^{3+}$ and at 3780, 4370, 4750, 7960 and 9130 cm^{-1} for $\mathbf{4}^{5+}$. These bands are essentially solvent independent in a range of solvents from CD_3NO_2 (D_{op} = 1.909) to $(CD_3)_2SO$ (D_{op} = 2.182). Spectral deconvolution for mixed-

Table 4. Near-Infrared Bands in CD_3CN

complex	E_{abs} (cm^{-1}) (ϵ (M^{-1} cm^{-1})) $\Delta\bar{\nu}_{1/2}$ (cm^{-1}) (in italics)				
	band I	band II	band III	band IV	band V
$[(bpy)_2(Cl)Os^{III}(4,4'\text{-bpy})Os^{III}(Cl)(bpy)_2]^{4+}$ (**1**$^{4+}$)	4200 (450)[b] *1000*	6100 (620)[b] *500*			
$[(bpy)_2(Cl)Os^{III}(4,4'\text{-bpy})Os^{II}(Cl)(bpy)_2]^{3+}$ (**1**$^{3+}$)	4200 (310)[b] *600*	6000 (450)[b] *1200*	*a*	*a*	*a*
$[(bpy)_2(Cl)Os^{III}(pz)Os^{III}(Cl)(bpy)_2]^{4+}$ (**2**$^{4+}$)	4250 (400)[b] *1000*	6350 (500)[b] *300*			
$[(bpy)_2(Cl)Os(pz)Os(Cl)(bpy)_2]^{3+}$ (**2**$^{3+}$)	2620 (2300) *1150*	3590 (1340)[b] *835*	4960 (980)[b] *650*	6000 (250) *2000*	7500 (250) *2500*
$[(tpy)(bpy)^{III}Os(4,4'\text{-bpy})^{III}Os(bpy)(tpy)]^{6+}$ (**3**$^{6+}$)	4300 (670)[b] *1000*	5200 (900)[b] *1200*			
$[(tpy)(bpy)Os^{III}(4,4'\text{-bpy})Os^{II}(bpy)(tpy)]^{6+}$ (**3**$^{5+}$)	4300 (380)[b] *~1500*	5200 (450)[b] *~1700*	*c*	~7700 (~150)[d]	~11 000 (~200)[d]
$[(tpy)(bpy)Os(pz)Os(bpy)(tpy)]^{6+}$ (**4**$^{6+}$)	4100 (550)[b] *500*	5540 (500)[b] *700*			
$[(tpy)(bpy)Os(pz)Os(bpy)(tpy)]^{5+}$ (**4**$^{5+}$)	3780 (900)[b] *560*	4370 (240) *3430*	4750 (420)[b] *550*	7960 (530) *1090*	9130 (1030) *2100*
$[Os(bpy)_2(Cl)(4,4'\text{-bpy})]^{2+}$	4070 (65)[b] *300*	6730 (120)[b] *930*			
$[Os(bpy)_2(Cl)(pz)]^{2+}$	4240 (200)[b] *400*	6330 (250)[b] *1100*			
$[Os(tpy)(bpy)(4,4'\text{-bpy})]^{3+}$	4280 (220)[b] *350*	6130 (300)[b] *850*			
$[Os(tpy(bpy)(pz)]^{3+}$	4200 (230)[b] *400*	5250 (190)[b] *940*			

[a] Very broad, overlapping absorptions. No maxima could be identified. [b] $d\pi \rightarrow d\pi$ interconfigurational bands. [c] Could not be clearly identified. [d] Very broad bands. Barely observable maxima could be identified. Calculation of $\Delta\bar{\nu}_{1/2}$ was not possible.

valence dimers **1**$^{3+}$ and **3**$^{5+}$ could not be reliably conducted because of the extremely broad, overlapping bands that appear in the near-infrared (see below).

The spectrum of **1**$^{2+}$ in the near-infrared is featureless while $d\pi \rightarrow d\pi$ bands at $d\pi^5$ Os^{III} appear at 4200 and 6100 cm^{-1} for **1**$^{4+}$.[13,28] These narrow bands are of low intensity and appear at the same energies for $[Os(bpy)_2(Cl)(py)]^{2+}$ and **1**$^{3+}$, although at half the intensity. The increasing absorptivity above 10 500 cm^{-1} in this spectrum is the tail of a low-energy MLCT band. In this spectrum, there is a broad, featureless band extending from ~5000 to 10 000 cm^{-1} with $\epsilon \sim 200-250$ M^{-1} cm^{-1}.

In the spectrum of **2**$^{2+}$, the tail of the $Os^{II}(d\pi) \rightarrow pz(\pi^*)$ band at ~13100 cm^{-1} appears above 11000 cm^{-1}, but the spectrum is otherwise featureless. In the near-infrared spectrum of **2**$^{4+}$, $d\pi \rightarrow d\pi$ bands appear at 4250 and 6350 cm^{-1} of the same energy and shape and twice the intensity of analogous bands for $[Os(bpy)_2(Cl)(py)]^{2+}$. The spectrum of **2**$^{3+}$ is complex. Overlapping bands appear at ~3000 cm^{-1} which are deconvoluted into separate bands at 3590 and 2620 cm^{-1}. There are a band at 5000 cm^{-1} of $\epsilon \sim 1000$ M^{-1} cm^{-1} and broad overlapping bands having maxima at <5800 and ≥ 7300 cm^{-1} with $\epsilon < 300$ M^{-1} cm^{-1}. As noted previously, a $d\pi \rightarrow p^*(pz)$ "triplet" band appears at 8900 cm^{-1} ($\epsilon \sim 1100$ M^{-1} cm^{-1}). The increase in absorption past 10 300 cm^{-1} is due to tailing from MLCT absorption in the visible. The ν(pz) stretch at 1599 cm^{-1} is also shown in this spectrum.

In the spectrum of **3**$^{6+}$, $d\pi \rightarrow d\pi$ bands appear at 4300 cm^{-1} ($\epsilon = 670$ M^{-1} cm^{-1}) and 5200 cm^{-1} ($\epsilon = 900$ M^{-1} cm^{-1}). They appear at 4100 cm^{-1} ($\epsilon = 550$ M^{-1} cm^{-1}) and 5540 cm^{-1} ($\epsilon = 500$ M^{-1} cm^{-1}) for **4**$^{6+}$. In the spectrum of **3**$^{5+}$, $d\pi \rightarrow d\pi$ bands appear at 4300 cm^{-1} ($\epsilon = 380$ M^{-1} cm^{-1}) and 5200 cm^{-1} ($\epsilon = 450$ M^{-1} cm^{-1}). There is a broad region of absorption from 5500 to 12 5000 cm^{-1} ($\epsilon \sim 150-200$ M^{-1} cm^{-1}) with barely apparent maxima at ~7700 and ~11000 cm^{-1}. For **4**$^{5+}$, $d\pi \rightarrow d\pi$ bands of enhanced intensity appear at 3800 cm^{-1} ($\epsilon = 1240$ M^{-1} cm^{-1}) and 4700 cm^{-1} ($\epsilon = 930$ M^{-1} cm^{-1}). In addition, an intense band appears at 9000 cm^{-1} ($\epsilon = 1420$ M^{-1} cm^{-1}) with $\Delta\bar{\nu}_{1/2} = 3400$ cm^{-1} which can be resolved into separate components at 7960 and 9130 cm^{-1}. When the sample is cooled to 240 K in CD_3CN, this band grows in intensity (by ~10%) and sharpens, with $\Delta\bar{\nu}_{1/2} = 2800$ cm^{-1}. An additional, broad feature appears beneath the $d\pi \rightarrow d\pi$ bands at ~5000 cm^{-1} which, upon deconvolution, appears at 4370 cm^{-1}.

Discussion

The goal of this study was the continued exploration of the localized-to-delocalized, mixed-valence transition in ligand-bridged Os complexes. Earlier work has shown that, in analogous complexes of Ru, such as *cis,cis*-$[(bpy)_2(Cl)Ru(pz)Ru(Cl)(bpy)_2]^{3+}$,[3] there are localized oxidation states and low barriers to intramolecular electron transfer. Neglecting the effect of electronic delocalization, the classical barrier to electron transfer in symmetrical complexes is $\lambda/4$, where λ is the sum of the intramolecular (λ_i) and solvent (λ_o) reorganizational energies.[1h]

$$\lambda = \lambda_i + \lambda_o \qquad (1)$$

In the 5d Os analogues, there is a greater d orbital extension. This enhances electronic coupling and, with the use of N_2 or pz as bridges, provides experimental access to the localized-to-delocalized transition region. In the present study, the focus was on the Os analogue of *cis,cis*-$[(bpy)_2(Cl)Ru(pz)Ru(Cl)(bpy)_2]^{3+}$ [3c] and the related derivative $[(tpy)(bpy)Os(pz)Os(bpy)(tpy)]^{5+}$. The 4,4′-bpy-bridged analogues were also studied as a point of reference, since electronic coupling across this bridge is less and they provide models for localization.

$[(bpy)_2(Cl)Os(4,4'\text{-bpy})Os(Cl)(bpy)_2]^{3+}$ (1^{3+}) and $[(tpy)(bpy)Os(4,4'\text{-bpy})Os(bpy)(tpy)]^{5+}$ (3^{5+}). Attempts to grow

(28) (a) Sen, J.; Taube, H. *Acta Chem. Scand.* **1979**, *A33*, 125. (b) Taube, H. *Pure Appl. Chem.* **1979**, *51*, 901. (c) Creutz, C.; Chou, M. H. *Inorg. Chem.* **1987**, *26*, 2995. (d) Dubicki, L.; Frguson, J.; Krautz, E. R.; Lay, P. A.; Maeder, M.; Taube, H. *J. Phys. Chem.* **1984**, *88*, 3940. (e) Aràneo, A.; Mercati, G.; Morazzoni, F.; Napoletano, T. *Inorg. Chem.* **1977**, *16*, 1196.

crystals of $\mathbf{3}^{5+}$ as the PF_6^- salt from CH_3CN/Et_2O resulted instead in the separate crystallization of $\mathbf{3}^{4+}$ and $\mathbf{3}^{6+}$. Crystals of $\mathbf{3}^{6+}$ were of poor X-ray quality and were unsuitable for structure determination.

In the structure of $\mathbf{3}^{4+}$, the rings in μ-4,4′-bpy are coplanar. There is literature precedent for this,[29] although it is not a universal case.[30] The coplanar orientation allows maximum overlap through the π orbitals of the ring system.

Bond lengths in $\mathbf{3}^{4+}$ can be compared to those in $[(NH_3)_5Os^{III}(pz)Os^{III}(NH_3)_5]^{6+}$ [31] and $[(NH_3)_5Ru^{III}(pz)Ru^{III}(NH_3)_5]^{6+}$.[32] In the former, Os−N(pz) is 2.101(7) Å, and in the latter, Ru−N(pz) is 2.115(1) Å. In $\mathbf{3}^{4+}$, Os−N(μ-4,4′-bpy) is 2.115(6) Å. The Os^{II}−N bond lengths in $\mathbf{3}^{4+}$ are comparable to Os^{III}−N(pz) because of dπ−π*(pz) back-bonding. These bond lengths are shorter than typical Os−N single-bond lengths. For example, Os^{II}−$N(NH_3)$ is 2.123(7)−2.139(6) Å in $[(CH_3CN)(NH_3)_4Os(N_2)Os(NH_3)_4(NCCH_3)]^{5+}$.[33] This points to a role for back-bonding. Os−N(bpy) and Os−N(tpy) bond lengths in $\mathbf{3}^{4+}$ compare well with those in $[Os^{II}(tpy)(bpy)(OH_2)](CF_3SO_2)_2$[34a] and $[Ru^{II}(tpy)(bpy)(OH_2)](ClO_4)_2$.[34b]

There is nothing unusual in the properties of $\mathbf{1}^{2+}/\mathbf{1}^{3+}/\mathbf{1}^{4+}$ or $\mathbf{3}^{4+}/\mathbf{3}^{5+}/\mathbf{3}^{6+}$. The UV−vis absorption spectra of $\mathbf{1}^{2+}$ and $\mathbf{3}^{4+}$ are dominated by $Os^{II} \rightarrow$ bpy, 4,4′-bpy MLCT bands and are half the sum of the spectra of $\mathbf{1}^{2+}$, $\mathbf{1}^{4+}$ and $\mathbf{3}^{4+}$, $\mathbf{3}^{6+}$, respectively. In the NIR spectra of $\mathbf{1}^{3+}$ and $\mathbf{3}^{5+}$, the expected two bands from d$\pi \rightarrow$ dπ interconfigurational transitions within the dπ^5(Os^{III}) core are observed, Table 4. Their IT bands are weak and broad, and it was not possible to deconvolute them reliably. A third IT band is expected and is probably hidden beneath the lowest energy MLCT band at higher energy which tails into the near-infrared.

$[(bpy)_2(Cl)Os(pz)Os(Cl)(bpy)_2]^{3+}$ ($\mathbf{2}^{3+}$) and $[(tpy)(bpy)Os(pz)Os(bpy)(tpy)]^{5+}$ ($\mathbf{4}^{5+}$). The properties of the pz-bridged complexes are more difficult to rationalize. They display an added complexity in behavior which is becoming characteristic of the localized-to-delocalized transition. It is convenient to review and analyze the properties of $\mathbf{2}^{3+}$ and $\mathbf{4}^{5+}$ separately and then to discuss them more generally.

$[(bpy)_2(Cl)Os(pz)Os(Cl)(bpy)_2]^{3+}$ ($\mathbf{2}^{3+}$). In this ion, the appearance of interconfigurational d$\pi \rightarrow$dπ bands at Os^{III}, at 3590 and 4960 cm^{-1}, provides markers for Os^{III}.[8,28] These bands are red-shifted and more intense than those of $\mathbf{2}^{4+}$, consistent with significant electronic coupling across the pz bridge. As discussed elsewhere, this provides an orbital basis for mixing IT character into these normally weak d$\pi \rightarrow$ dπ transitions, which enhances their intensities.[8,28]

The appearance of ν(pz) in the spectrum of $\mathbf{2}^{3+}$ (but not in that of $\mathbf{2}^{2+}$ or $\mathbf{2}^{4+}$) is also consistent with the description Os^{III}−Os^{II}, at least on the time scale for near infrared light absorption. This is approximately the period of the vibration or $\sim 2.0 \times 10^{-14}$ s (~20 fs). This provides an upper limit for the electron transfer rate constant and $k_{ET} < 5 \times 10^{13}\ s^{-1}$.

Even though the appearance of ν(pz) provides direct experimental evidence for localization, the ν(bpy) bands from 1400 to 1500 cm^{-1} are averaged. This can be seen clearly in the IR band comparisons in Figure 4. This is not just a solution effect. Similar observations were made in KBr pellets.

The intensity of ν(pz) with $\epsilon = 2600\ M^{-1}\ cm^{-1}$ is unusually high when compared with $\epsilon = 600\ M^{-1}\ cm^{-1}$ for *cis*-$[Os^{II}(bpy)_2(Cl)(pz)]^+$.[10] Even though oxidation states are localized, extensive d$\pi(Os^{III})$−π,π*(pz)−d$\pi(Os^{II})$ mixing may result in the coupling of charge-transfer character into this normally symmetrical ring-stretching mode. This is a non-Condon effect with a coupling between the nuclear coordinates of the bridge and the coordinates of the transferring electron.

Electronic transitions for this ion extend from the near-infrared into the infrared. In addition to ν(pz) at 1599 cm^{-1}, there is evidence for six bands having an electronic origin. Assuming that the band at 8930 cm^{-1} can be assigned to the lowest energy MLCT "triplet" transition, five bands remain to be assigned.

On the basis of an analysis presented elsewhere,[3a,8,9] which assumes localized oxidation states, five bands are expected, two from the d$\pi \rightarrow$ dπ transitions mentioned above and three from IT transitions due to electronic excitation from the separate dπ_1, dπ_2, and dπ_3 orbitals at Os^{II} to the vacancy in dπ_3 at Os^{III}. On the basis of this analysis, the bands labeled I, IV, and V in Figure 5B can be assigned to IT(1), IT(2), and IT(3). The underlying transitions are as follows: d$\pi_3(Os^{II}) \rightarrow$ d$\pi_3(Os^{III})$, IT(1); d$\pi_2(Os^{II}) \rightarrow$ d$\pi_3(Os^{III})$, IT(2); d$\pi_1(Os^{II}) \rightarrow$ d$\pi_3(Os^{III})$, IT(3). (Because of spin−orbit coupling, the Cartesian character of the d_{xy}, d_{xz}, and d_{yz} orbitals at Os^{III} are highly mixed.[35]) The remaining two bands, II and III, arise from the interconfigurational transitions $d\pi_1^2\, d\pi_2^2\, d\pi_3^1 \rightarrow d\pi_1^2\, d\pi_2^1\, d\pi_3^2$ and $d\pi_1^2\, d\pi_2^2\, d\pi_3^1 \rightarrow d\pi_1^1\, d\pi_2^2\, d\pi_3^2$.

Band shape parameters for the individual bands (labeled as I−V in Figure 5B and Table 4) following spectral deconvolution are listed in Table 4. The bandwidths for the bands assigned to IT transitions are noticeably broader than the d$\pi \rightarrow$ dπ bands. Nonetheless, in solvents ranging from CD_3NO_2 to $(CD_3)_2SO$, they are relatively solvent independent. This and the low-energy of IT(1), at 2620 cm^{-1}, are consistent with no or an insignificant contribution from the solvent to the absorption band energy with $\lambda_o \sim 0$ in eq 1.

The absence of a solvent dependence combined with localized oxidation states has been observed for other complexes.[8,9] These

(29) (a) Stang, P. J.; Olenyuk, B. *Acc. Chem. Res.* **1997**, *30*, 502. (b) Yaghi, O. M.; Li, H. *J. Am. Chem. Soc.* **1997**, *119*, 7013. (c) Shen, H.-Y.; Liao, D.-Z.; Jiang, Z.-H.; Yan, S.-P.; Sun, B.-W.; Wang, G.-L.; Yao, X.-K.; Wang, H.-G. *Polyhedron* **1998**, *17*, 1953. (d) Tong, M.-L.; Ye, B.-H.; Cai, J.-W.; Chen, X.-M.; Ng, S.-W. *Inorg. Chem.* **1998**, *37*, 2645. (e) Li, J.; Zeng, H.; Chen, J.; Wang, Q.; Wu, X. *Chem. Commun.* **1997**, 1213. (f) Yaghi, O. M.; Li, G. *Angew. Chem., Int. Ed. Engl.* **1995**, *34*, 207. (g) Chen, X.-M.; Tong, M.-L.; Luo, Y.-J.; Chen, Z.-N. *Aust. J. Chem.* **1996**, *49*, 835. (h) Maekawa, M.; Munakata, M.; Kuroda-Sowa, T.; Hachiya, K. *Inorg. Chim. Acta* **1995**, *232*, 231. (i) Lu, J.; Paliwala, T.; Lim, S. C.; Yu, C.; Niu, T.; Jacobson, A. J. *Inorg. Chem.* **1997**, *36*, 923. (j) Lu, J.; Yu, C.; Niu, T.; Paliwala, T.; Crisci, G.; Somosa, F.; Jacobson, A. J. *Inorg. Chem.* **1998**, *37*, 4637.

(30) (a) Yaghi, O. M.; Li, H. *J. Am. Chem. Soc.* **1995**, *117*, 10401. (b) Fujita, M.; Kwon, Y. J.; Washizu, S.; Ogura, K. *J. Am. Chem. Soc.* **1994**, *116*, 1151. (c) Yaghi, O. M.; Li, H.; Groy, T. L. *Inorg. Chem.* **1997**, *36*, 4292. (d) Tong, M.-L.; Chen, X.-M.; Yu, X.-L.; Mak, T. C. W. *J. Chem. Soc., Dalton Trans.* **1998**, 5. (e) Berkstein, K. D.; Hupp, J. T.; Stern, C. L. *J. Am. Chem. Soc.* **1998**, *120*, 12982.

(31) Molecular structure of $[(NH_3)_5Os^{III}(pz)Os^{III}(NH_3)_5]^{5+}$: Bino, A.; Lay, P. A.; Taube, H.; Wishart, J. F. *Inorg. Chem.* **1985**, *24*, 3969.

(32) Molecular structure of $[(NH_3)_5Ru^{III}(pz)Ru^{III}(NH_3)_5]^{5+}$: (a) Fürholz, U.; Bürgi, H.-B.; Wagner, F. E.; Stebler, A.; Ammeter, J. H.; Krausz, E.; Clark, R. J. H.; Stead, M. J.; Ludi, A. *J. Am. Chem. Soc.* **1984**, *106*, 121. (b) Fürholz, U.; Joss, S.; Bürgi, H.-B.; Ludi, A. *Inorg. Chem.* **1985**, *24*, 943.

(33) (a) Che, C.-M.; Lam, H.-W.; Tong, W.-F.; Lai, T.-F.; Lau, T.-C. *J. Chem. Soc., Chem. Commun.* **1989**, 1883. (b) Lam, H.-W.; Che, C.-M.; Wong, K.-Y. *J. Chem. Soc., Dalton Trans.* **1992**, 1411.

(34) (a) Molecular structure of $[Os^{II}(tpy)(bpy)(OH_2)](CF_3SO_2)_2$: Cheng, C.-C.; Goll, J. G.; Neyhart, G. A.; Welch, T. W.; Singh, P.; Thorp, H. H. *J. Am. Chem. Soc.* **1995**, *117*, 2970. (b) Molecular structure of $[Ru^{II}(tpy)(bpy)(OH_2)](ClO_4)_2$: Seok, W. K.; Kim, M. Y.; Yokomori, Y.; Hodgson, D. J.; Meyer, T. J. *Bull. Korean Chem. Soc.* **1995**, *16*, 619.

(35) Goodman, B. A.; Raynor, J. B. *Adv. Inorg. Chem. Radiochem.* **1970**, *13*, 135.

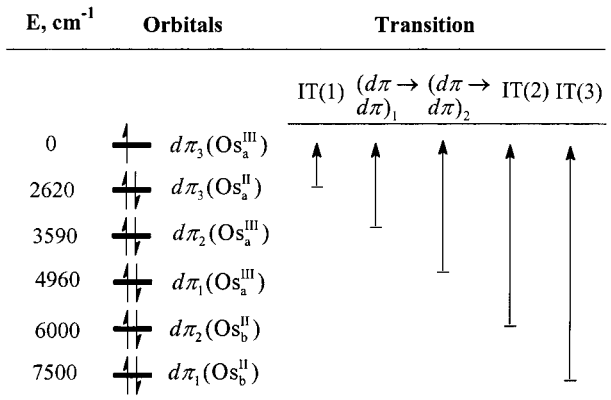

Figure 6. Band Energies and Assignments for $[(bpy)_2(Cl)Os_a^{III}(pz)Os_b^{II}(Cl)(bpy)_2]^{3+}$ in CD_3CN.

are the defining characteristics of the localized-to-delocalized, mixed-valence transition region. The absence of solvent coupling can be explained as a consequence of the time scale for intramolecular electron transfer. If electron transfer is rapid compared to the ~1 ps time scale for solvent dipole reorientation,[36] these motions become uncoupled from electron transfer because they are too slow. The solvent orientational polarization is averaged, appropriate to the delocalized charge distribution $Os^{II.5}-Os^{II.5}$ even though the complex is localized because electron transfer is still coupled to intramolecular vibrations. The IT bands remain narrow at −38.5 °C, showing that the solvent remains averaged at this temperature as well.

The assignment of near-infrared bands is illustrated in the energy level diagram in Figure 6. In the diagram, the $d\pi(Os^{III})$ and $d\pi(Os^{II})$ orbitals are mixed with π(pz) and π^*(pz) bridge orbitals. The π,π^*(pz) character in these orbitals promotes $d\pi(Os^{III})-d\pi(Os^{II})$ mixing across the bridge. The final orbitals that result, which include $Os^{III}-Os^{II}$ mixing, are labeled $d\pi(Os_a^{II})$ and $d\pi(Os_b^{III})$ with the subscript a or b the label across the bridge.

IT(1) is the most intense feature in the spectrum. It is a transition from $d\pi_3(Os^{II})$ to $d\pi_3(Os^{III})$. Spin−orbit coupling at Os^{III} imparts considerable d_{xy}, d_{xz}, and d_{yz} character to all three $d\pi(Os^{III})$ orbitals.[19,20] Defining the $Os^{III}-pz-Os^{II}$ axis as the *z* axis, $d\pi_3(Os^{III})$ must have considerable *z* character, oriented toward the pyrazine plane to maximize mixing with π,π^*(pz). The remaining bands at 6000 and 7500 cm^{-1} are IT(2) and IT(3). They originate in the transitions $d\pi_2(Os^{II}) \rightarrow d\pi_2(Os^{III})$, and $d\pi_1(Os^{II}) \rightarrow d\pi_1(Os^{II})$. They have *z* character but are less strongly mixed with π,π^*(pz) than in $[(bpy)_2(Cl)Os^{III}(pz)Ru^{II}(NH_3)_5]^{4+}$, where the orbital coupling scheme is different. The pattern of IT band intensities, IT(1) > IT(2), IT(3), is in contrast to the pattern IT(1) < IT(2), IT(3) observed for *trans,trans*-$[(tpy)(Cl)_2Os^{III}(N_2)Os^{II}(Cl)_2(tpy)]^+$, where the orbital coupling scheme is also different.[9]

The low-energy orbital pathway for $Os^{II} \rightarrow Os^{III}$ electron transfer in $\mathbf{2}^{3+}$ is $d\pi_3(Os^{II}) \rightarrow d\pi_3(Os^{III})$, and this pathway dominates thermal electron transfer as well. The alternate pathways $d\pi_2(Os^{II}) \rightarrow d\pi_3(Os^{III})$ and $d\pi_1(Os^{II}) \rightarrow d\pi_3(Os^{III})$ are not important because they result in the initial formation of interconfigurational excited states at Os^{III}, $(d\pi_1)^2(d\pi_2)^1(d\pi_3)^2$ or $(d\pi_1)^1(d\pi_2)^2(d\pi_3)^2$ and are uphill by 3590 and 4960 cm^{-1}.

The optical analogue of this electron transfer pathway is IT(1). As noted above, the absence of solvent coupling to the IT transition helps to explain the relatively low energy for IT(1).

The energies of the IT and $d\pi \rightarrow d\pi$ bands should be related as $E_{IT}(2) \sim E_{IT}(1) + E_{d\pi \rightarrow d\pi}(1)$ and $E_{IT}(3) \sim E_{IT}(1) + E_{d\pi \rightarrow d\pi}$-

Table 5. Calculated Values for H_{DA} for $\mathbf{2}^{3+}$ and $\mathbf{4}^{5+}$ in CD_3CN[a]

	H_{DA} (cm^{-1})			
complex	H_{DA} (1)	H_{DA} (2)	H_{DA} (3)	H_{DA} (total)
$[(bpy)_2(Cl)Os(pz)Os(Cl)(bpy)_2]^{3+}$ ($\mathbf{2}^{3+}$)	247	163	203	613
$[(tpy)(bpy)Os(pz)Os(bpy)(tpy)]^{5+}$ ($\mathbf{4}^{5+}$)	178	201	417	796

[a] These are minimum values (see text). The labels 1−3 correspond to bands I, IV, and V for $\mathbf{2}^{3+}$ in Table 4 and to bands II, IV, and V for $\mathbf{4}^{5+}$.

(2). For IT(2) and IT(3), the experimental values, 6000 and 7500 cm^{-1}, are close to the calculated values of 6210 and 7480 cm^{-1}.

For Gaussian-shaped absorption bands, it is possible to calculate the electronic resonance energy arising from $Os^{III}-Os^{II}$ electronic coupling by using eq 2,[1h] where ϵ_{max} is the molar

$$H_{DA} = \sqrt{\frac{4.2 \times 10^{-4} \epsilon_{max} \Delta\bar{\nu}_{1/2} E_{abs}}{d^2}} \qquad (2)$$

extinction coefficient (in M^{-1} cm^{-1}) at the absorption maximum, E_{abs} (in cm^{-1}), for the spectrum scaled as $\int \epsilon(\bar{\nu})\, d\bar{\nu}/\bar{\nu}$,[1h] $\Delta\bar{\nu}_{1/2}$ is the bandwidth at half-height (in cm^{-1}), and *d* is the metal−metal separation distance (in Å).

The results of the spectral deconvolution procedure were summarized in Table 4. H_{DA} values for each IT band were calculated by using eq 2 and these band shape parameters are listed in Table 5. In these calculations, *d* was taken as 6.9 Å.[31,37] Consequently, the H_{DA} *values are lower limits* since electronic coupling across the bridge decreases the charge-transfer distance compared to the geometrical distance.[38]

For $\mathbf{2}^{3+}$, the exchange energy arising from the lowest energy $Os^{III}-Os^{II}$ orbital pathway, $d\pi_3(Os^{II}) \rightarrow d\pi_3(Os^{III})$, is $H_{DA} \geq 247$ cm^{-1}. The quantities $H_{DA}(2)$ and $H_{DA}(3)$ are the exchange energies in the mixed-valence excited states with the configuraitons $d\pi_1^2 d\pi_2^1 d\pi_3^2$ and $d\pi_1^1 d\pi_2^2 d\pi_3^2$ at Os^{III}.

In the classical limit, k_{ET} is given by

$$k_{ET} = \nu_{ET} \exp(-\Delta G^*/RT) \qquad (3)$$

where ν_{ET} is the frequency factor for electron transfer and ΔG^* the free energy of activation. Neglecting electronic delocalization, $\Delta G^* = \lambda/4$ in the classical limit.[39,40] If the solvent component, λ_o, is averaged, $\lambda_o \sim 0$. There is still a contribution to λ_o from dispersive interactions with the solvent. $\lambda \sim \lambda_i$, where λ_i is the intramolecular reorganizational energy. It includes the sum of λ's for all coupled, low-frequency metal−ligand vibrations. On the basis of this analysis, λ is given by eq 4,

$$\lambda \sim \sum_l S_l \hbar\omega_l \qquad (4)$$

where S_l and $\hbar\omega_l$ ($=h\nu_l$) are the electron−vibrational coupling constants and quantum spacings and the sum is over the coupled vibrations, *l*. *S* is

(36) (a) Horng, M. L.; Gardechi, J. A.; Papazyan, A.; Maroncelli, M. *J. Phys. Chem.* **1995**, *99*, 17311. (b) Fleming, G. R.; Cho, M. *Annu. Rev. Phys. Chem.* **1996**, *47*, 109.
(37) Mayoh, B.; Day, P. *Inorg. Chem.* **1974**, *13*, 2273.
(38) (a) Hupp, J. T.; Dong, Y.; Blackburn, R. L.; Lu, H. *J. Phys. Chem.* **1993**, *97*, 3278. (b) Bublitz, G. U.; Boxer, S. G. *Annu. Rev. Phys. Chem.* **1997**, *48*, 213. (c) Reimers, J. R.; Hush, N. S. *J. Am. Chem. Soc.* **1995**, *117*, 1302.
(39) (a) Marcus, R. A. In *Tunneling in Biological Systems*; Chance, B., DeVault, D. C., Frauenfelder, H., Marcus, R. A., Schrieffer, J. R., Sutin, N., Eds; Academic Press: New York, 1979; p 109. (b) Marcus, R. A. *J. Chem. Phys.* **1956**, *24*, 979. (c) Marcus, R. A. *J. Chem. Phys.* **1956**, *24*, 966.

related to the reduced mass (M) and change in equilibrium displacement (ΔQ_e) by

$$S = {}^1/_2(M\omega/\hbar)(\Delta Q_e)^2 \quad (5)$$

When electron delocalization is included, ΔG^* is related to λ and $H_{DA}(1)$ as in eq 6.[40b]

$$\Delta G^* = \frac{\lambda}{4} - H_{DA}(1) + \frac{[H_{DA}(1)]^2}{\lambda} \quad (6)$$

Upon the inclusion of a single, coupled high-frequency mode, the rate constant expression becomes

$$k_{ET} = \nu_{ET}\sum_{\upsilon'}[\exp(-S)]\frac{S^{\upsilon'}}{\upsilon'!}\exp\left\{-\frac{\frac{\lambda}{4} - H_{DA}(1) + \frac{[H_{DA}(1)]^2}{\lambda}}{RT}\right\} \quad (7)$$

This equation includes contributions through a series of vibrational channels from initial level $\upsilon = 0$ to a series of final levels υ' for the high-frequency mode. Although the IR analysis points to averaged ν(bpy) vibrations, there is a contribution from ν(pz). Given the magnitude of ΔG^* (see below), only the $\upsilon = 0 \rightarrow \upsilon' = 0$ channel can contribute significantly, given the quantum spacing of 1599 cm^{-1}, and the only important channel for this mode is $\upsilon = 0 \rightarrow \upsilon' = 0$. In this limit

$$k_{ET} = \nu_{ET}[\exp(-S)]\exp\left\{-\frac{\frac{\lambda}{4} - H_{DA}(1) + \frac{[H_{DA}(1)]^2}{\lambda}}{RT}\right\} \quad (8)$$

With use of the experimental values in Tables 4 and 5, $\Delta G^* = 408$ cm^{-1} (0.05 eV) for $\mathbf{2}^{3+}$. Even in the absence of solvent coupling, a barrier is expected to exist to electron transfer from coupled, low-frequency Os−Cl and Os−N modes. The magnitude of $H_{DA}(1)$ is sufficient that electron transfer occurs in the adiabatic regime and ν_{ET} is dictated by the dynamics of the coupled vibrations.[39,40] By assuming $\exp(-S) \sim 1$ and $\nu_{ET} = 10^{13}$ s^{-1}, $k_{ET}(CH_3CN, 298\ K) = 8.3 \times 10^{10}$ s^{-1} ($\tau_{ET} \sim 12.0$ ps) for $\mathbf{2}^{3+}$. This value is a lower limit because the H_{DA} value used to calculate ΔG^* is a lower limit. The calculated value of τ_{ET} is longer than the time scale for solvent dipole reorientation, which is ~0.26 ps in CH_3CN, and is inconsistent with solvent averaging.[36,41]

The coupled Os−Cl and Os−N modes are of low frequency. On the basis of existing crystallographic data,[9] the changes in equilibrium displacement are expected to be small and tunneling transitions from levels below the barrier may play an important role, decreasing the barrier and increasing k_{ET}.[9]

From this analysis, $H_{DA}(1) \geq 247$ cm^{-1} and $\lambda = 2620$ cm^{-1}. ($=E_{IT}(1)$, band I in Table 5). This is consistent with localization since $2H_{DA}(1)/\lambda \geq 0.18$.[1,2] It also shows that there is considerable electronic delocalization in $\mathbf{2}^{3+}$. In this region the Born−Oppenheimer approximation is no longer applicable.[4a,b,d,f,5a−c] The energy levels and wave functions are dependent on both nuclear and electronic coordinates.

For the mixed-valence equilibrium in eq 9, $\Delta G^\circ_{COM} = \Delta E_{1/2} = -0.19$ eV. Electronic delocalization in the ground state of the mixed-valence ion accounts for $2H_{DA}(1) \gtrsim 494$ cm^{-1} or ~32% of the total.

$$[(bpy)_2(Cl)Os^{III}(pz)Os^{III}(Cl)(bpy)_2]^{4+} + [(bpy)_2(Cl)Os^{II}(pz)Os^{II}(Cl)(bpy)_2]^{2+} \rightleftharpoons 2[(bpy)_2(Cl)Os^{III}(pz)Os^{II}(Cl)(bpy)_2]^{3+} \quad (9)$$

[(tpy)(bpy)Os(BL)Os(tpy)(bpy)]$^{5+}$. In $\mathbf{3}^{3+}$ with BL = 4,4′-bpy, there is clear evidence for localized oxidation states in the UV−visible and IR spectra, but unfortunately, there is little information in the near-infrared spectrum. Broad bands appear for the lowest two of three expected IT bands with evidence for band maxima at ~8000 and ~11000 cm^{-1}, with $\epsilon \sim 200$ M^{-1} cm^{-1}.

For $\mathbf{4}^{5+}$, there is evidence for the influence of through-bridge electronic coupling in the magnitude of $\Delta E_{1/2}$ and the perturbed MLCT spectra in the visible region, Figure 3D. There is also evidence for localization in the appearance of interconfigurational $d\pi \rightarrow d\pi$ (d^5 Os^{III}) bands at 3780 and 4750 cm^{-1}. The second marker for localization is the appearance of the intense ν(pz) band at 1594 cm^{-1}. As for $\mathbf{2}^{3+}$, this band is unusually intense, with $\epsilon = 2020$ M^{-1} cm^{-1}, again perhaps due to the mixing of charge-transfer character into the symmetrical stretch.

Interpretation of the ν(bpy) and ν(tpy) bands from 1400 to 1500 cm^{-1} is far more ambiguous because of the overlap of these bands. For $\mathbf{3}^{5+}$, with BL = 4,4′-bpy, the pattern of bands is simply half the sum of the $\mathbf{3}^{4+}$ and $\mathbf{3}^{6+}$ bands (Figure 4C). For $\mathbf{4}^{5+}$, the same number of bands appear as in the averaged spectrum, ${}^1/_2(\mathbf{4}^{4+} + \mathbf{4}^{6+}$ bands), but there are significant changes in band energies and intensities as described in Results, with different bands being affected in different ways. We have made no attempt to analyze this spectrum quantitatively. The changes that are observed may be a consequence of electronic coupling and the onset of dynamical effects, with the electron-transfer time scale approaching that for ν(bpy) and ν(tpy). This may be a case similar to that described by Ito and Kubiak for a series of pyrazine-bridged clusters.[42] By making systematic ligand variations, they were able to control k_{ET} for intramolecular electron transfer and observe line broadening and coalescence in ν(CO) metal carbonyl marker bands in the infrared spectra.

The near-infrared spectrum of $\mathbf{4}^{5+}$ can also be assigned by application of the energy level diagram in Scheme 1. In this case, IT(1) at ~4370 cm^{-1} (band II in Figure 5D) is completely overlapped with $d\pi-d\pi$ bands at 3780 and 4750 cm^{-1} (bands I and III). IT(2) and IT(3) appear at 7960 and 9130 cm^{-1} as an overlapped pair of bands (bands IV and V). Because of the limitations imposed by the analysis, the reliability of bandwidths derived from the band shape analysis for both $\mathbf{2}^{3+}$ and $\mathbf{4}^{5+}$ is questionable. Nonetheless, the widths of bands assigned to IT transitions are noticeably greater than those for the $d\pi-d\pi$ bands in both cases (Table 4). On the basis of these assignments and the relationships $E_{IT}(2) \sim E_{IT}(1) + E_{d\pi\rightarrow d\pi}(1)$ and $E_{IT}(3) \sim E_{IT}(1) + E_{d\pi\rightarrow d\pi}(2)$, $E_{IT}(2) = 8150$ cm^{-1} and $E_{IT}(3) = 9120$ cm^{-1}, in good agreement with the experimental values of 7960 and 9130 cm^{-1}.

(40) (a) Marcus, R. A.; Sutin, N. *Biophys. Biochim. Acta* **1985**, *811*, 265. (b) Sutin, N. *Prog. Inorg. Chem.* **1983**, *30*, 411. (c) Newton, M. D.; Sutin, N. *Annu. Rev. Phys. Chem.* **1984**, *35*, 437. (d) Sutin, N. *Acc. Chem. Res.* **1982**, *15*, 275. (e) Marcus, R. A. *Rev. Mod. Phys.* **1993**, *65*, 599. (f) Barbara, P. F.; Meyer, T. J.; Ratner, M. A. *J. Phys. Chem.* **1996**, *100*, 13148.

(41) (a) Barbara, P. F.; Jarzeba, W. *Adv. Photochem.* **1990**, *15*, 1. (b) Calef, D. F.; Wolynes, P. G. *J. Phys. Chem.* **1983**, *87*, 3387.

(42) (a) Ito, T.; Hamaguchi, T.; Nagino, H.; Yamaguchi, T.; Washington, J.; Kubiak, C. P. *Science* **1997**, *277*, 660. (b) Vlcek, A., Jr. *Chemtracts: Inorg. Chem.* **1998**, *11*, 127. (c) Ito, T.; Hamaguchi, T.; Niqino, H.; Yamaguchi, T.; Kido, H.; Zavarine, I. S.; Richmond, T.; Washington, J.; Kubiak, C. P. *J. Am. Chem. Soc.* **1999**, *121*, 4625.

(43) Haga, M.; Matsumura-Inoue, T.; Yamabe, S. *Inorg. Chem.* **1987**, *26*, 4148.

From the H_{DA} values in Table 5, $H_{DA}(1) = 178$ cm^{-1}. On the basis of this analysis, the contribution of mixed-valence, electronic delocalization to $\Delta G°_{COM} = -0.16$ eV for the comproportionation equilibrium

$$[(tpy)(bpy)Os^{III}(pz)Os^{III}(bpy)(tpy)]^{6+} + [(tpy)(bpy)Os^{II}(pz)Os^{II}(bpy)(tpy)]^{4+} \rightleftharpoons 2[(tpy)(bpy)Os^{III}(pz)Os^{II}(bpy)(tpy)]^{5+} \quad (10)$$

is $\sim 2H_{DA}(1) \gtrsim 356$ cm^{-1} or $\sim$27% of the total. Since $H_{DA}(1) \geq 178$ cm^{-1} and $\lambda = 4370$ cm^{-1}, $2H_{DA}(1)/\lambda \geq 0.08$.

Conclusions

In prevailing theories of mixed-valence compounds, the internal electronic structure depends on a balance. One factor is the tendency to localize oxidation states, which maximizes differences in intramolecular structure and solvent polarization. The other is the tendency to maximize electronic delocalization and with it the electronic resonance energy. Quantitative application of these theories typically relies on making simplifying assumptions about electronic structure and, typically, use of an averaged mode approximation for the coupled vibrations.

The polypyridyl complexes described here reveal how complex a complete description must be to capture the full nuances of the underlying molecular and electronic structures. These are complex molecules with complex electronic structures. Electronic coupling occurs through three separate dπ−dπ orbital interactions, all of which rely on π,π^*(pz) mixing. For Os, low symmetry and spin−orbit coupling impart through-bridge axial character to all three as evidenced by the comparable magnitudes of $2H_{DA}$ for the three IT bands. Electronic coupling leads to a perturbation with Os^{III} character mixed into Os^{II}, but it is not sufficient to cause delocalization. The magnitudes of H_{DA} in the mixed-valence ground states of $\mathbf{2}^{3+}$ and $\mathbf{4}^{5+}$ are only $\gtrsim$247 and $\gtrsim$178 cm^{-1}, respectively. These values are less than, but approach significant fractions of, the reorganizational energies of $\sim$2600 and $\sim$4400 cm^{-1}. In these molecules, electronic delocalization energies are not great but the effect of delocalization is significant because of the low barriers to electron transfer.

The effect of delocalization on the coupled vibrations is to decrease the changes in equilibrium displacement in the normal modes and, with these, the electron transfer barrier. The coupling of the various molecular motions to electronic structure and how they contribute to the barrier are highly idiosyncratic.

The time scale for solvent reorientations is relatively slow. If the time scale for electron transfer is more rapid, these motions are no longer dynamically coupled and assume an orientation appropriate to the averaged charge distribution, $Os^{II.5}$−$Os^{II.5}$.

Different vibrations couple in different ways. Low-frequency Os−Cl and Os−N vibrations, which respond to changes in oxidation state, and for which $\Delta Q_e \neq 0$, are the probable origin of the residual electron-transfer barrier. There are medium frequency "spectator" vibrations, such as ν(pz) and ν(bpy), which are "on or off" or averaged depending on whether electron transfer is fast or slow compared to their characteristic time scales. For $\mathbf{3}^{+}$, ν(bpy) averaging occurs and, given the small shifts between oxidation states (5−7 cm^{-1}), electron transfer must be more rapid than the $\sim$10 ps time scale for coalescence.[42] The ν(pz) marker is more rapid. The band can only appear if there is a local electronic asymmetry on the time scale of near infrared absorption of $\sim$20 fs. From these two values k_{ET} can be bracketed as 10^{11} s$^{-1} \leq k_{ET} \leq 2 \times 10^{13}$ s^{-1}.

On the basis of the high absorptivity of ν(pz) for $\mathbf{2}^{3+}$ and $\mathbf{4}^{5+}$, this mode may also have coupled charge-transfer character.

Both $\mathbf{2}^{3+}$ and $\mathbf{4}^{5+}$ can be described as being at the localized-to-delocalized transition, not appropriately described by either limiting case. Even so, there are differences between them. For $\mathbf{2}^{3+}$, the bpy modes from 1300 to 1400 cm^{-1} are averaged. For $\mathbf{4}^{5+}$, the bpy and tpy modes in this region are perturbed, not averaged. Also, as measured by IT band energies, λ is greater for all three IT bands by 1600−2000 cm^{-1}.

There are other mixed-valence Os complexes that exhibit the ambiguity of properties that is a hallmark of the localized-to-delocalized, mixed-valence transition. The near-infrared spectra of $\mathbf{4}^{5+}$ and $[(bpy)_2Os(BiBzIm)Os(bpy)_2]^{3+}$ (BiBzIm = 2,2′-bibenzimidazolate) are strikingly similar. The latter shows a structured IT band centered at 8180 cm^{-1} ($\epsilon = 1800$ M^{-1} cm^{-1}), an IT band at 4800 cm^{-1} ($\epsilon = 500$ M^{-1} cm^{-1}), and the expected two interconfigurational dπ−dπ bands at 5450 cm^{-1} ($\epsilon = 960$ M^{-1} cm^{-1}) and 4400 cm^{-1} ($\epsilon = 300$ M^{-1} cm^{-1}).[43] $\Delta E_{1/2}$ is 180 mV. For $[(NC)_5Os(pz)Os(CN)_5]^{5-}$, ν(pz) appears at 1582 cm^{-1}, which also points to localization.[44]

We propose that these molecules constitute a new class of mixed-valence molecules, Class II−III, that lie in a domain between what is conventionally described as localized and delocalized. The characteristic features of this class are that oxidation states, or valences, are localized because of vibrational coupling but that intramolecular electron transfer is sufficiently rapid that solvent orientational motions are uncoupled. Because of this, *these molecules literally have properties associated with both Class II and Class III*.

Acknowledgment. We thank the National Science Foundation for funding this research under Grants CHE-9321413 and CHE-9503738.

Supporting Information Available: Infrared spectra for $\mathbf{1}^{2+}$−$\mathbf{4}^{6+}$ in the region 1400−1500 cm^{-1}, a table of infrared band energies for $\mathbf{1}^{2+}$−$\mathbf{4}^{6+}$, and a listing of final positional parameters, along with their standard deviations as estimated from the inverse matrix, a table of anisotropic thermal parameters, extended tables of bond distances, angles, and torsion angles, and packing diagrams for $\mathbf{3}^{4+}$. This material is available free of charge via the Internet at http://pubs.acs.org.

IC9907765

(44) Hornung, F. M.; Baumann, F.; Kaim, W.; Olabe, J. A.; Slep, L. D.; Fiedler, J. *Inorg. Chem.* **1998**, *37*, 311.